



# A multi-model CMIP6 study of Arctic sea ice at 127 ka: Sea ice data compilation and model differences

Masa Kageyama<sup>1,\*</sup>, Louise C. Sime<sup>2,\*</sup>, Marie Sicard<sup>1,\*</sup>, Maria-Vittoria Guarino<sup>2,\*</sup>, Anne de Vernal<sup>3</sup>, David Schroeder<sup>4</sup>, Ruediger Stein<sup>5,6</sup>, Irene Malmierca-Vallet<sup>2</sup>, Ayako Abe-Ouchi<sup>7</sup>, Cecilia Bitz<sup>8</sup>, Pascale Braconnot<sup>1</sup>, Esther C. Brady<sup>9</sup>, Jian Cao<sup>10</sup>, Matthew A. Chamberlain<sup>11</sup>, Danny Feltham<sup>4</sup>, Chuncheng Guo<sup>12</sup>, Allegra N. LeGrande<sup>13</sup>, Gerrit Lohmann<sup>5</sup>, Katrin J. Meissner<sup>14</sup>, Laurie Menviel<sup>14</sup>, Polina Morozova<sup>15</sup>, Kerim H. Nisancioglu<sup>16,17</sup>, Bette L. Otto-Bliesner<sup>9</sup>, Ryouta O’ishi<sup>7</sup>, Silvana Ramos Buarque<sup>18</sup>, David Salas y Melia<sup>18</sup>, Sam Sherriff-Tadano<sup>7</sup>, Julianne Stroeve<sup>19</sup>, Xiaoxu Shi<sup>5</sup>, Bo Sun<sup>10</sup>, Robert A. Tomas<sup>9</sup>, Evgeny Volodin<sup>20</sup>, Nicholas K. H. Yeung<sup>14</sup>, Qiong Zhang<sup>21</sup>, Zhongshi Zhang<sup>22,11</sup>, and Tilo Ziehn<sup>23</sup>

<sup>1</sup>Laboratoire des Sciences du Climat et de l’Environnement, Institut Pierre Simon Laplace, Université Paris-Saclay, 91191 Gif-sur-Yvette Cedex, France

<sup>2</sup>British Antarctic Survey, Cambridge, UK

<sup>3</sup>Departement des sciences de la Terre et de l’atmosphère, Universite du Quebec, Montreal, Canada

<sup>4</sup>Centre for Polar Observation and Modelling, Department of Meteorology, University of Reading, Reading, UK

<sup>5</sup>Alfred Wegener Institute Helmholtz Centre for Polar and Marine Research, Bremerhaven, Germany

<sup>6</sup>MARUM - Center for Marine Environmental Sciences and Faculty of Geosciences, University of Bremen, Germany

<sup>7</sup>The University of Tokyo, Japan

<sup>8</sup>Department of Atmospheric Sciences, University of Washington, USA

<sup>9</sup>National Center for Atmospheric Research, Boulder, USA

<sup>10</sup>Nanjing University of Information Science and Technology, Nanjing, China

<sup>11</sup>CSIRO Oceans and Atmosphere, Hobart, TAS, Australia

<sup>12</sup>NORCE Norwegian Research Centre, Bjerknes Centre for Climate Research, Bergen, Norway

<sup>13</sup>NASA Goddard Institute for Space Studies, 2880 Broadway, New York, NY 10025, USA

<sup>14</sup>Climate Change Research Centre, ARC Centre of Excellence for Climate Extremes, The University of New South Wales, Sydney, Australia

<sup>15</sup>Institute of Geography, Russian Academy of Sciences, Staromonetny L. 29, Moscow, 119017, Russia

<sup>16</sup>Department of Earth Science, University of Bergen, Bjerknes Centre for Climate Research, Allégaten 41, 5007, Bergen, Norway

<sup>17</sup>Centre for Earth Evolution and Dynamics, University of Oslo, Oslo, Norway

<sup>18</sup>Centre National de Recherches Météorologiques (CNRM), Université de Toulouse, Météo-France, CNRS (Centre National de la Recherche Scientifique), Toulouse, France

<sup>19</sup>University College London, UK

<sup>20</sup>Marchuk Institute of Numerical Mathematics, Russian Academy of Sciences, ul. Gubkina 8, Moscow, 119333, Russia

<sup>21</sup>Department of Physical Geography, Stockholm University, Stockholm, Sweden

<sup>22</sup>Department of Atmospheric Science, School of Environmental Studies, China University of Geoscience (Wuhan), Wuhan, China

<sup>23</sup>CSIRO Oceans and Atmosphere, Aspendale, VIC, Australia

\*The first four authors equally contributed to the manuscript

**Correspondence:** Masa Kageyama (Masa.Kageyama@lsce.ipsl.fr)

**Abstract.** The Last interglacial (LIG) is a period with increased summer insolation at high northern latitudes, which results in strong changes in the terrestrial and marine cryosphere. Understanding the mechanisms for this response via climate modelling and comparing the models' representation of climate reconstructions is one of the objectives set up by the Paleoclimate Modelling Intercomparison Project for its contribution to the sixth phase of the Coupled Model Intercomparison Project. Here 5 we analyse the results from 16 climate models in terms of Arctic sea ice. The mean pre-industrial to LIG reduction in minimum sea ice area reaches 50% (multi-model mean LIG area is 3.20 mill. km<sup>2</sup>, compared to 6.46 mill. km<sup>2</sup> for the PI). On the other hand there is little change for the maximum sea ice area (which is 15-16 mill. km<sup>2</sup> for both the PI and the LIG). To evaluate the model results we synthesize LIG sea ice data from marine cores collected in the Arctic Ocean, Nordic Seas and northern North Atlantic. The reconstructions for the northern North Atlantic show year-round ice free conditions, and most 10 models yield results in agreement with these reconstructions. Model-data disagreement appear for the sites in the Nordic Seas, close to Greenland, and at the edge of the Arctic Ocean. The northernmost site with good chronology, for which a sea ice concentration larger than 75% is reconstructed even in summer, discriminates those models which simulate too little sea ice. However, the remaining models appear to simulate too much sea ice over the two sites south of the northernmost one, for 15 which the reconstructed sea ice cover is seasonal. Hence models either under or over estimate sea ice cover for the LIG, and their bias does not appear to be related to their bias for the pre-industrial period. Drivers for the inter-model differences are: different phasing of the up and down short-wave anomalies over the Arctic ocean, associated with differences in model albedo; possible cloud property differences, in terms of optical depth; LIG ocean circulation changes which occur for some, but not all, LIG simulations. Finally, we note that inter-comparisons between the LIG simulations and simulations for future climate with 20 with moderate (1% per year) CO<sub>2</sub> increase show a relationship between LIG sea ice and sea ice simulated under CO<sub>2</sub> increase around the years of doubling CO<sub>2</sub>. The LIG may therefore yield insight into likely 21st century Arctic sea ice changes using these LIG simulations.

*Copyright statement.* TEXT

## 1 Introduction

The Last Interglacial (LIG) was the last time global temperature was substantially higher than the pre-industrial at high 25 northern latitudes. It is important in helping us understand warm climates sea ice and climate dynamics (Otto-Bliesner et al., 2013; Capron et al., 2017; Otto-Bliesner et al., 2017; Fischer et al., 2018). Stronger LIG spring and summertime insolation contributed to this warmth, as well as feedbacks amplifying the initial insolation signal, in particular feedbacks related to the marine and land cryosphere. Previous climate model simulations of the LIG, forced by appropriate greenhouse gas (GHG) and orbital changes, have failed to capture the observed high temperatures at higher latitudes (Malmierca-Vallet et al., 2018; 30 Masson-Delmotte et al., 2011; Otto-Bliesner et al., 2013; Lunt et al., 2013). Models used during the previous Coupled Model Intercomparison Project 5 (CMIP5) disagree on the magnitude of Arctic sea ice retreat during the LIG: the diversity of sea

ice behaviour across models was linked to the spread in simulated surface temperatures and in the magnitude of the polar amplification (Otto-Bliesner et al., 2013; Lunt *et al.*, 2013; IPCC, 2013). However it was difficult to compare some of the LIG simulations because they were not all run using identical protocol. These studies thus highlighted the need of a systematic approach to study the role of Arctic sea ice changes during the LIG.

Coupled Model Intercomparison Projects (CMIPs) coordinate and design climate model protocols for the past, present and future climates, and have become an indispensable tool to facilitate our understanding of climate change (IPCC, 2007, 2013; Eyring et al., 2016). The Paleoclimate Model Intercomparison Project 4 (PMIP4) is one of the individual Model Intercomparison Projects which is taking part in CMIP6 (Kageyama et al., 2018). Within this framework, a common experimental protocol for Last Interglacial (LIG) climate simulation was developed by Otto-Bliesner et al. (2017). CMIP models differ among each other in their physical formulation, numerical discretization and code implementation. However this CMIP6-PMIP4 LIG standard protocol facilitates model inter-comparison work.

Alongside a previous lack of a common experimental protocol, our ability to evaluate CMIP models has previously been hindered by difficulties in determining LIG sea ice extent from marine core evidence (*e.g.* Otto-Bliesner et al., 2013; Sime et al., 2013; Malmierca-Vallet et al., 2018; Stein et al., 2017). Planktonic foraminifers assemblages that include a subpolar component suggest reduced sea ice in the Arctic Ocean (Nørgaard-Pedersen et al., 2007; Adler et al., 2009). Microfauna found in LIG marine sediments recovered from the Beaufort Sea Shelf, an area characterized by ice-free conditions during summers today, support ice-free conditions during that time as well; these indicate that more saline Atlantic water was present on the Beaufort Shelf, suggesting reduced perennial Arctic sea ice during some part of the LIG (Brigham-Grette and Hopkins, 1995). On the other hand, a reconstruction of LIG Arctic sea ice changes based on sea ice biomarker proxies (see below for details), suggests that the central part of the LIG Arctic Ocean remained ice covered throughout the year while a significant reduction of LIG sea ice occurred across the Barents Sea continental margin (Stein et al., 2017). On the modelling side, no previous coupled climate model has simulated an ice-free Arctic during the LIG (Otto-Bliesner et al., 2006; Lunt *et al.*, 2013; Otto-Bliesner et al., 2013; Stein et al., 2017).

Here we address the question of LIG Arctic sea ice by providing a new marine core synthesis. Additionally, the CMIP6-PMIP4 LIG experimental protocol developed by Otto-Bliesner et al. (2017) provides the systematic framework to enable us to examine the question of the simulation of LIG Arctic sea ice using a multi-model approach. This is important given the current level of interest in the ability of climate models to accurately represent key Arctic climate processes during warm periods, including sea ice formation and melting. We compare the LIG Arctic sea ice simulated by each model against our new data synthesis, and investigate why different models show different Arctic sea ice behaviour.

## 2 Materials and methods

### 2.1 Current Arctic sea ice

Our main objective is to investigate LIG sea-ice. However, a quick assessment of the sea ice simulated in the reference state, *i.e.* the pre-industrial control experiment (referred to *piControl* in the CMIP6 terminology, and PI in this manuscript) was

65 necessary. In the absence of extensive sea ice data for the PI period, we used data for a recent period before the current sea ice cover significant decrease. We use the NOAA Optimum Interpolation version 2 data (Reynolds et al., 2002) for the period 1982 to 2001. The sea-ice data in this data set is obtained from different satellite and in-situ observations. We have used the monthly time series, at a resolution of  $1^{\circ}$ . This data set is termed 'NOAA\_OI\_v2' in the rest of this document.

## 2.2 Marine records of LIG Arctic sea ice

70 We focus here on records of sea ice from marine cores. Table 1 provides a summary of LIG sea ice information and data obtained from marine sediment cores collected in the Arctic Ocean, Nordic Seas and northern North Atlantic. South of  $78^{\circ}\text{N}$ , the records show ice-free conditions. Most of these sea ice records are derived from quantitative estimates of sea-surface parameters based on dinoflagellate cysts (dinocysts). North of  $78^{\circ}\text{N}$  the sea-ice related records are rare and different types of indicators were used. In addition to dinocysts, the records are based on biomarkers linked to phototrophic productivity in sea 75 ice and on foraminifers and ostracods that both provide indication on water properties and indirectly on sea ice (de Vernal et al., 2013b). Between  $78$  and  $87^{\circ}\text{N}$ , the faunal data have been interpreted as indicating seasonal sea-ice cover conditions during the LIG.

Among sea-ice cover indicators, dinocyst assemblages have been used as quantitative proxy based on the application of the modern analogue technique applied to a standardized reference modern data base developed from surface sediment samples 80 collected at middle to high latitudes of the Northern Hemisphere (de Vernal et al., 2005; de Vernal et al., 2005b, 2013b, 2019). The sea-ice estimates from dinocysts used here are from different studies (see references in Table 1) and reconstructions based the new database including 71 taxa and 1968 stations (de Vernal et al., 2019). The reference sea ice data used for calibration are the monthly 1955-2012 average of the National Snow and Ice Data Center NSIDC (Walsh et al., 2016). The results are expressed in term of annual mean of sea-ice cover concentration or as the number of months with  $>50\%$  of sea-ice. The error 85 of prediction for sea-ice concentration is  $\pm 12\%$  and that of sea-ice cover duration through the year is  $\pm 1.5$  months/yr. Such values are very close to the interannual variability in areas occupied by seasonal sea-ice cover (cf. de Vernal et al., 2013b).

Our biomarker approach for sea ice reconstruction is based on the determination of a highly branched isoprenoid (HBI) with 25 carbons (C25 HBI monoene = IP25) (Belt et al., 2007). This biomarker is only biosynthesized by specific diatoms living in the Arctic sea ice (Brown et al., 2014), meaning the presence of IP25 in the sediments is a direct proof for the presence 90 of past Arctic sea ice. Meanwhile, this biomarker approach has been used successfully in numerous studies dealing with the reconstruction of past Arctic sea ice conditions during late Miocene to Holocene times (for a review, see Belt, 2018). By combining the sea ice proxy IP25 with (biomarker) proxies for open-water (phytoplankton productivity such as brassicasterol, dinosterol or a specific tri-unsaturated HBI (HBI-III)), the so-called PIP25 index has been developed (Müller et al., 2011; Belt et al., 2015; Smik et al., 2016). Based on a comparison ("calibration") PIP25 data obtained from surface sediments with 95 modern satellite-derived (spring) sea ice concentration maps (Müller et al., 2011; Xiao et al., 2015; Smik et al., 2016), the PIP25 approach may allow a more semi-quantitative reconstruction of present and past Arctic Ocean sea ice conditions from marine sediments, i.e., estimates of spring sea ice concentration (or in the central Arctic probably more the summer situation due to light limitations for algae growth in the other seasons). Based on these data one may separate "permanent to extended

sea ice cover" (>0.75), "seasonal sea ice cover" (0.75-0.1), perhaps with sub-groups "ice-edge" (0.75-0.5) and "less/reduced sea ice" (0.5-0.1), and "ice-free" (<0.1). For pros and cons of this approach we refer to a most recent review by Belt (2018).

Based on several IP25/PIP25 records obtained from central Arctic Ocean sediment cores (see Fig. 1 for core locations and Table 1 for data), perennial sea ice cover has probably existed during the LIG in the Central Arctic, whereas along the Barents Sea continental margin, influenced by the inflow of warm Atlantic Water, sea ice was significantly reduced Stein et al. (2017). However, Stein et al. (2017) emphasize that the PIP25 records obtained from the central Arctic Ocean cores indicating a perennial sea ice cover have to be interpreted cautiously as the biomarker concentrations are very low to absent (see Belt 2018 for further discussion). The productivity of algal material (ice and open water) must have been quite low, so that (almost) nothing reached the seafloor or is preserved in the sediments, and there must have been periods during the LIG when some open-water conditions occurred, since subpolar foraminifers and coccoliths were found in core PS51/038 and PS2200 (Stein et al., 2017). It is however unclear whether these periods equate to more than a month per year of open water (or seasonal ice conditions). This explains why some sites show both seasonal and perennial interpretations at the same site. The reader is referred to the original publications (Table 1) for more information on these data. Furthermore and importantly, a new revised <sup>230</sup>Th chronology of late Quaternary sequences from the central Arctic Ocean (Hillaire-Marcel et al., 2017) questions the age model of some of the data listed in Table 1. Thus, further verification of age control is still needed and the data from the central Arctic Ocean should be interpreted with caution. We have therefore marked the chronological control as "uncertain" for these cores, while the chronological control is good for cores outside the Central Arctic.

The information given by the different types of sea ice indicators shows that care should be taken when comparing them with model results. We have used the qualitative information given in Table 1, taking into account the threshold given in this table. Indeed, for instance, "perennial sea ice cover" does not automatically mean 100% sea ice cover, or a sea ice concentration (SIC) of 1.0. It means rather that there is sea ice, but not necessarily at a concentration of 100%, over the core site throughout the year (*i.e.* the summer season is not totally ice-free). Most qualitative reconstructions cite a threshold of 75%, which we have therefore used in our model-data comparison. We have also used the quantitative mean annual sea ice reconstructions. Finally, similar to studies for future climate, we have considered the Arctic to be ice-free when, on any given month, the total area of sea ice is less than 1 million km<sup>2</sup>. This means that some marine core sites could remain ice covered for the summer, but the Arctic would nevertheless remain technically ice-free.

## 125 2.3 CMIP6-PMIP4 Models

The last Coupled Model Intercomparison Project Phase 5 (CMIP5) collected climate simulations performed with 60 different numerical models by 26 research institutes around the world (IPCC, 2013). The follow-on CMIP6 archive, to be completed in 2020, is expected to gather model outputs from over 30 research institutes. Of these, currently fifteen models have run the CMIP6-PMIP4 LIG simulation (Table 2). We present results here from all these models.

130 Table 2 provides an overview of the models used in this study. They are state-of-the-art coupled general circulation models (GCM) and Earth System Models (ESM) simulating the atmosphere, ocean, sea ice and land surface processes dynamics with a varying degree of complexity across them. These 16 models have been developed for several years by individual institutes

across the world and, in the context of CMIP6, are used in the same configuration to simulate seamlessly past, present and future climate. We have added the results from the LOVECLIM Earth System Model of Intermediate Complexity, which can  
135 be used for longer simulations.

Table 2 shows for each model: model denomination, physical core components, horizontal and vertical grid specifications, details on prescribed vs interactive boundary conditions, relative publication for an in-depth model description, and LIG simulation length (spin-up and production runs).

## 2.4 PMIP4 LIG (*lig127k*) simulation protocol

140 Results shown here are from main Tier 1 LIG simulation, from the standard CMIP6-PMIP4 LIG experimental protocol (Otto-Bliesner et al., 2017). The prescribed LIG (*lig127k*) protocol differs from the CMIP6 pre-industrial (PI) simulation protocol in astronomical parameters and the atmospheric trace greenhouse gas concentrations (GHG). LIG astronomical parameters are prescribed according to orbital constants (Berger and Loutre, 1991), and atmospheric trace GHG concentrations are based on ice core measurements. Table 3 from Otto-Bliesner et al. (2017) summarizes the protocol. All models followed this protocol,  
145 except CNRM-CM6-1 for which the most important forcings for the LIG, i.e. the astronomical parameters, have been imposed at the recommended values, but the GHG have been kept at their pre-industrial values of 284.3170 ppm for CO<sub>2</sub>, 808.2490 ppb for CH<sub>4</sub> and 273.0211 ppb for N<sub>2</sub>O. All other boundary conditions, including solar activity, ice sheets, aerosol emissions and etc., are identical to PI protocol. Both the Greenland and Antarctica ice sheets are known to have shrunk during the interglacial, with different timings, and therefore taking PI characteristics for the *lig127k protocol* is an approximation, in particular for the  
150 Antarctic ice sheet which was possibly smaller than PI at that time (Otto-Bliesner et al., 2017). The Greenland ice sheet likely reached a minimum at around 120 ky BP and was probably still close to its PI size at 127ka BP. Given the dating uncertainties and the difficulty for models to include the largest changes in ice sheets for 127 ka BP, i.e. changes in West Antarctica, the choice of the PMIIP4 working group on interglacials was to use the PI ice sheets as boundary conditions for the Tier 1 PMIP4-CMIP6 experiments presented here, and to foster sensitivity experiments to ice sheet characteristics at a later stage. In terms of  
155 the Greenland ice sheet, the approximation is considered as quite good and ideal for starting transient experiments through the whole interglacial.

LIG simulation were initialized either from a previous LIG run, or from the standard CMIP6 protocol pre-industrial simulations, using constant 1850 GHGs, ozone, solar, tropospheric aerosol, stratospheric volcanic aerosol and land use forcing.

160 Although PI and LIG spin-ups vary between the models, most model groups aimed to allowed the land and oceanic masses to attain approximate steady state *i.e.* to reach atmospheric equilibrium and to achieve an upper-oceanic equilibrium. LIG production runs are all between 100-200 years long, which is generally within the appropriate length for Arctic sea ice analysis (Guarino et al., 2020).

165 The LIG orbital parameters result in modifications of the definitions of the months and seasons (in terms of start and end dates within a year). Since daily data was not available for all models to re-compute LIG-specific monthly averages, we have corrected these averages using the method of Bartlein and Shafer (2019). Unless otherwise specified, we use these results adjusted for the LIG calendar throughout this manuscript.

## 2.5 The CMIP6 *1pctCO<sub>2</sub>* protocol

We compare the response to the *lig127k* forcings to idealised forcings for future climate. We have chosen to use the *1pctCO<sub>2</sub>* simulation from the CMIP6 DECK (Diagnostic, Evaluation and Characterization of Klima Eyring et al., 2016). These simulations start from the PI (*piControl*) experiment and the atmospheric CO<sub>2</sub> concentration is gradually increased by 1% per year for at least 150 years, i.e. 10 years after atmospheric CO<sub>2</sub> quadrupling.

## 3 Results: simulated Arctic sea ice

Since all LIG production runs are at least 100 years in length, all model results are averaged over at least 100 years. We refer to the multi-model mean throughout as the MMM. We consider both the sea ice area (SIA), defined as the sum, over all northern hemisphere ocean cells, of the sea ice concentration  $\times$  the cell area and the sea ice extent (SIE), defined as the sum of the areas of ocean cells where the sea ice concentration is larger than 0.15. Both quantities are used in sea ice studies, SIE has been used widely in IPCC AR5 (Vaughan et al., 2013), while SIA tends to be used more for CMIP6 analyses (e.g. SIMIP Community, 2020).

### 3.1 PI sea ice

For the present-day we have satellite and in-situ observations with which to evaluate the models. The use of present-day sea ice data implies that we might expect the simulated PI sea ice to be generally somewhat larger than the observed mean. Indeed the atmospheric CO<sub>2</sub> levels for the years for which we chose the observation data set (1982 to 2001) were between 340 and 370 ppm, to be compared to the PI level of 280 ppm. Figure 2 shows the mean seasonal cycle of the Arctic sea-ice extent simulated for the PI and LIG alongside the observed Arctic sea-ice extent.

The summer minimum monthly MMM SIA for the PI is  $6.46 \pm 1.41$  mill. km<sup>2</sup>, compared to the observed 1981 to 2002 mean of 5.65 mill km<sup>2</sup>. In terms of SIE, the summer minimum for PI is  $(8.89 \pm 1.41)$  mill. km<sup>2</sup>, to be compared to the observed 7.73 mill. km<sup>2</sup>. Interestingly this MMM PI area and extent is a little larger than the 1981–2002 area. The majority of the simulations show a realistic representation of the geographical extent for the summer minimum (Figure 3, Table 4), with nine out of sixteen models showing a slightly smaller area compared to the present-day observations, and seven showing an overestimated area. LOVECLIM, EC-Earth, FGOALS-g3, GISS-E2-1-G and INMCM4-8 clearly simulate too much ice (Table 4). The other models generally exhibit realistic PI summer minimum ice conditions. The detail of the geographical distribution of sea ice for the models, the MMM and the NOAA\_OI\_v2 data sets (Fig. 3) confirms the results in terms of Arctic sea-ice extent. Overestimations appear to be due to too much sea ice being simulated in the Barents-Kara area (LOVECLIM, FGOALS-g3, GISS-E2-1-G), in the Nordic Seas (EC-Earth, FGOALS-g3) and in Baffin Bay (LOVECLIM, INMCM4-8, EX-Earth). MIROC-ES2L performs rather poorly for the PI, with insufficient ice close to the continents. The other models are generally matching the 0.15 isoline from the NOAA\_OI\_v2 data set in a realistic manner. The winter maximum monthly MMM areas show little difference between the present day and PI simulated areas. The MMM PI area is  $15.16 \pm 1.90$  mill

km<sup>2</sup>, compared to the observed 1981 to 2002 mean of 14.44 mill km<sup>2</sup>. For both the summer and winter, the simulations and observations mostly agree on the month that the minimum and maximum are attained: July-August for the minimum; and 200 Jan-Feb for the maximum for every model).

Before we carry out the comparison between model results and sea ice cover reconstructions for the LIG period, we compare the results of the models for PI to the observations at the reconstruction sites (Figure 4 for the comparison of annual mean sea ice concentrations and Figure 5, top, for winter and summer). Models generally overestimate sea ice cover at the three northernmost sites, in summer, and in annual mean and over the seven northernmost sites for the winter season. Those sites are 205 actually very close to the sea ice edge and the overestimation could correspond to the fact that the observations are for 1981 to 2002 period, already warmer than the pre-industrial one.

### 3.2 LIG sea ice

The models show a minimum monthly MMM SIA for the LIG of  $3.20 \pm 1.50$  mill. km<sup>2</sup>, and a maximum MMM SIA of  $15.95 \pm 2.61$  mill. km<sup>2</sup>. In terms of SIE, the minimum MMM extent is  $5.39 \pm 2.13$  mill. km<sup>2</sup>, while the maximum MMM extent 210 is equal to  $18.38 \pm 3.12$  mill. km<sup>2</sup>. Thus, compared to the PI results, there is a reduction of ca. 50% in the MMM minimum (summer) monthly SIA in the LIG results, and of nearly 40% in terms of SIE, but a slight increase in the winter monthly MMM SIA and SIE. Every model shows a reduction, often substantial, in summer sea ice between the PI and LIG.

There is a large amount of inter-model variability for the LIG SIA and SIE during the summer (Figure 6 and Table 4). Out of the sixteen models, one model, HadGEM3, shows a LIG Arctic Ocean free of sea ice in summer, i.e. with an SIE lower than 1 215 mill. km<sup>2</sup>. CESM2 and NESM3 show low SIA values (slightly above 2 mill. km<sup>2</sup>) in summer for the LIG simulation but their minimum SIE values are below 3 mill. km<sup>2</sup>. Both HadGEM3 and CESM2 realistically capture the PI Arctic sea ice seasonal cycle. On the other hand, NESM3 overestimates winter ice and the amplitude of the seasonal cycle in SIA and SIE, while 220 simulating realistic PI values for both SIA and SIE (Cao et al., 2018). This seasonal cycle is amplified in the LIG simulation, with an increase in SIA and SIE in winter and a decrease in summer, following the insolation forcing. Hence, the difference in the response of these models to LIG forcing in terms of sea ice does not appear to only depend on differences in PI sea ice representation.

For the winter only one (EC-Earth) out of the sixteen models show a (small) winter reduction in SIA between the PI and LIG and two show a LIG - PI decrease in SIE (Ec-Earth and ACCESS). All models therefore show a larger sea-ice area amplitude 225 for LIG than for PI, and the range of model results is larger for LIG than for PI. The summer season, but also the seasons of sea ice growth and decay, are therefore key to understand the behaviour of LIG sea ice and the inter-model differences, as will be confirmed in Section 4.

### 3.3 LIG model-data comparison

We limit our comparison to the sites for which the chronology is good. These cores mostly show ice free conditions in summer, except for the northernmost site (core PS92/039-2) which is at least 75% ice covered in summer (Figure 5, bottom left). 230 Two other sites at high latitude (PS213861 and PS93/006-1, for which sea ice has been reconstructed based on dinocysts

and IP25/PIP25), show summer conditions which are "probably ice free". Only four models simulate more than 75% sea ice concentration over the northernmost site but they also simulate more than 75% sea ice concentration over the two following sites (in descending order of latitudes) and EC-Earth simulates more than 75% sea ice concentration for another 4 sites for which the reconstructions show no sea ice. On the other hand, 10 models simulate no sea ice concentration at all over the reconstruction 235 sites in summer, and therefore probably overestimate the LIG summer sea ice reduction. From these reconstructions, we cannot distinguish the performance of the models simulating a strong reduction of sea ice from the model simulating a nearly total disappearance of summer sea ice in the Arctic. Apart from EC-Earth which simulates extensive sea ice cover for both periods, there does not appear to be a strong relationship between the PI and LIG model results over the data sites: models which 240 simulate sea ice cover over the three northernmost sites at the LIG do not necessarily simulate large sea ice concentrations over these sites for PI (e.g. LOVECLIM, AWIESM1 and AWIESM2).

For the winter season, the reconstructions show the four northernmost sites to be ice covered. The reconstructions for most other sites are qualitatively given as "nearly ice free all year round", or "ice free all year round". Model results are generally in agreement with the reconstructions for the three to four northernmost sites (Figure 5, bottom right). Most models simulate sea 245 ice over some of the sites characterized by "nearly ice free all year round" conditions and only one model (IPSLCM6) simulates sea ice cover over a site for which the reconstructions show ice free conditions. The model-data agreement is therefore quite good for the winter season. In this case, the model results for LIG appear to be related to their results for PI, with models simulating more sea ice for LIG being those simulating more sea ice for PI.

Figure 7 shows a quantitative model-data comparison in terms of annual mean sea ice concentration, which is the variable for which we have the highest number of reconstructions (Table 1). From this, we see that it is more difficult for the models 250 to realistically capture sea ice change over the core sites near Greenland, close to the sea ice edge. If we cross compare the observation-model match for each model for both the PI (Figure 4) and the LIG (Figure 7) then FGOALS-g3 and NESM3 have difficulties in accurately capturing sea-ice cover at the core site locations in the Nordic Seas, whilst AWIESM1 and NORESM1-F best display sea ice cover close to the sea ice edge near Greenland and in the Nordic seas sea for both time periods. It is these Nordic Seas sea ice edge differences (over the Table 1 core sites) that make the difference between the 255 simulation-data matches for each model.

#### 4 Discussion of model differences

Whilst we cannot yet definitely establish the most likely Arctic sea ice conditions during the LIG, we can investigate sea ice differences across models when we have sufficient model data. We have first performed this analysis for the three models for which we had sufficient data: CESM2, HadGEM3, and IPSLM6. These models each represent a distinct sea ice response to 260 the LIG forcing, *i.e.* summer sea ice concentration less than 0.15 everywhere (HadGEM3), significant summer sea ice retreat with concentration less than 0.8 in central Arctic (CESM2), modest summer sea ice retreat with a small area with sea ice concentration close to 1 in Central Arctic (IPSLCM6).

Sea ice formation and melting can be affected by a large number of factors inherent to the atmosphere and the ocean dynamics, alongside the representation of sea ice itself within the model (*i.e.* the type of sea ice scheme used). In coupled 265 models it can be extremely difficult to identify the causes of essentially coupled-model behaviour. Nevertheless, we discuss the short-wave (SW) surface energy balance, ocean and atmosphere circulations, and comment on cloudiness and albedo changes.

#### 4.1 Atmospheric energy budget differences

The atmospheric energy budget LIG – PI anomaly (Fig. 8) is negative in winter and strongly positive in summer, following the imposed insolation anomaly. These anomalies in total heat budget are dominated by the SW budget contribution from May 270 to August. We split the SW budget into the SWdown and SWup contributions. The SWup flux anomaly shown on Fig. 8 is counted positive downward, which means that the total SW budget (in black) is the sum of the SWdn contribution (in red) and the SWup contribution (in blue). On this figure, a positive SWup anomaly means that the SWup is less intense at LIG than at PI, hence contributing to an increase in the net SW flux.

For all the models, the total heat budget anomaly is due to (i) an increased downward SW flux in spring resulting from 275 the insolation forcing, and (ii) a decreased upward shortwave flux in summer, related to the decrease of the albedo due to the smaller sea-ice cover. During summer, this decrease in upward shortwave flux more than compensates the decrease in SWdn, which is maximum in August.

The summer anomaly reaches 80 W/m<sup>2</sup> in June for HadGEM3, 60 W/m<sup>2</sup> for IPSLCM6, 50 W/m<sup>2</sup> for CESM2. The differences between the model results are due to a different phasing of the SWdn and SWup anomalies for HadGEM3, compared to 280 the other two models: for HadGEM3, the two fluxes peak in June, while for CESM2 and IPSLCM6, the SWdn flux peaks in May and the SWup signal peaks in July, so that the anomaly in these fluxes partly compensate. HadGEM3 shows a larger net SW increase despite a SWdn anomaly which is smaller than for the other two models. On the other hand, HadGEM3's SWup component is stronger and always positive, which is different to the other two models which show a negative SWup contribution in April-May. These differences are associated with differences in albedo for the three models (Fig. 9). HadGEM3's sea 285 ice and Arctic ocean albedos are always smaller than those simulated by IPSLCM6 and CESM2 and the difference is larger for LIG than for PI. The albedo simulated by HadGEM3 in May and June is particularly low compared to the two other models, which explains why the SWup component peaks earlier. The albedo LIG–PI anomalies over the whole Arctic show that the sea-ice albedo feedback is most effective in HadGEM3.

In terms of cloudiness, IPSLCM6 shows differences in the properties of clouds, in terms of optical depth, between PI and 290 LIG, but this could not be investigated, due to a lack of data (thus far), for the other models. Thus we cannot tell if LIG–PI anomalies in SWdn fluxes, *i.e.* differences between HadGEM3's and CESM2 flux also have a contribution due to cloud changes.

The comparison to other model results (Fig. 10) confirm that the behaviour of HadGEM3 is unusual in terms of energy 295 budget. It is the only model in which the anomalies in SWup and SWdn are exactly in phase and produce a much larger anomaly in total heat budget, while in other models those anomalies are not in phase and partly compensate each other.

## 4.2 Ocean and atmosphere circulation differences

Changes in Arctic sea ice related to ocean heat transport have been found for the CESM large ensemble (Auclair and Tremblay, 2018). The differences can then be amplified by the sea-ice albedo feedbacks. We check this in our models by calculating long-term means of the maximum meridional stream function at 26°N for the PI and LIG simulations. These are 19.5 and 18.7 for

300 CESM2, 15.6 and 15.8 Sv for HadGEM3, and 12.9 and 10.4 for IPSLCM6. Thus, the CESM2 and HadGEM3 models exhibit an AMOC that is almost unchanged between PI and LIG, while in the IPSLCM6 model the AMOC weakens. This implies that a reduced northward oceanic heat transport could prevent sea ice loss in the central Arctic in some but not all models (see also Stein et al., 2017).

Some differences in the response of sea ice to LIG forcing therefore appear to be due either to differences in atmospheric 305 response (HadGEM3 vs IPSL-CM6 and CESM2), similar to mechanisms found for current sea ice decline (*e.g.* He et al. (2019); Olonscheck et al. (2019)) or to changes in ocean heat transport (CESM2 vs IPSLCM6). But while AMOC changes partially explain the differences found between IPSL (more sea ice in central Arctic) and CESM2 and HadGEM3 (less sea ice in central Arctic), they do not explain differences between ice-free and ice-covered conditions in HadGEM3 and CESM2.

Differences in atmospheric circulation changes could also explain difference in sea ice response to LIG forcings. We therefore 310 investigate LIG - PI anomalies in sea level pressure (Fig. 11). Most models simulate a decrease in summer mean sea level pressure largely encompassing the Arctic ocean and adjacent continents. This decrease is not as strong over the Nordic Seas than over the Arctic and this local heterogeneity over the Nordic Seas is model-dependent. However, the anomaly in atmospheric circulation is more zonal over the Nordic Seas and northern North Atlantic in HadGEM3 than in CESM2 or IPSLCM6, so that differences in atmospheric circulation are probably not causing more warm air to enter the Arctic for HadGEM3 and 315 are therefore not the cause of HadGEM3 being so warm over the Arctic. The mean sea level pressure winter anomaly is characterized by a deepening or the Icelandic low for all models except NESM3.

Other factors which remain to be investigated include clouds and ocean heat uptake in the Arctic in the different models, for example, as a function of stratification.

## 4.3 Transient CO<sub>2</sub> forced responses: LIG vs transient 1pctCO<sub>2</sub>

320 The LIG has higher insolation than PI at high northern latitudes during spring and summer, and less significant changes in winter insolation. This is distinct from the increased GHG which is the dominant forcing for future climates. However, since sea ice minimum occurs in summer, it is of interest to consider possible relationships between CMIP6 model responses for the LIG and those for the transient *1pctCO<sub>2</sub>* experiments. Twelve models have the LIG, PI and *1pctCO<sub>2</sub>* simulations available. These include models with large, small and intermediate responses in sea-ice for the LIG.

325 Figure 12 suggests that there is indeed such a relationship between the summer sea-ice concentration decreases for LIG and the averages from years 50 to 70 of the transient *1pctCO<sub>2</sub>* simulations : the models which respond strongly at LIG also respond strongly for the *1pctCO<sub>2</sub>* forcing, and the model with the smallest response for LIG (INMCM4-8) has the smallest response to the *1pctCO<sub>2</sub>* forcing. The relationship shown in Figure 12 does not last for later periods in the *1pctCO<sub>2</sub>* runs, when

the winter sea-ice is also affected by the increased greenhouse gas forcing. This implies inter-comparisons between the LIG  
330 simulation, and simulations with moderate CO<sub>2</sub> increase (during the transition to high CO<sub>2</sub> levels), should be investigated.

## 5 Conclusions

The Last Interglacial (LIG) was the last time global temperature was substantially higher than the pre-industrial at high northern  
latitudes (Otto-Bliesner et al., 2013; Capron et al., 2017; Otto-Bliesner et al., 2017; Fischer et al., 2018; Otto-Bliesner et al.,  
335 2020). To help understand the role of Arctic sea ice in these changes, we present a new synthesis of LIG sea ice information  
using marine core data collected in the Arctic Ocean, Nordic Seas and northern North Atlantic - and compare this to PMIP4-  
LIG simulations.

Our synthesis shows that south of 79°N in the Atlantic and Nordic seas the LIG was definitely seasonally ice-free. These  
southern sea ice records provide quantitative estimates of sea-surface parameters based on dinoflagellate cysts (dinocysts).  
North of 79°N the sea-ice related records are more difficult to obtain and interpret. However, the core at 81.5°N brings evidence  
340 of summer being probably seasonally ice free during the LIG from two indicators: dinocysts and IP25/PIP25. The northernmost  
core with good chronology is located at 81.9°N and shows evidence of substantial (> 75%) sea ice concentration all year round.  
Other cores, with debated chronologies, have not been used for model-data comparisons in the present study.

Model results from sixteen models show a multi model mean (MMM) summer SIA LIG of  $3.20 \pm 1.29$  mill. km<sup>2</sup>, and a  
winter monthly MMM area of  $15.95 \pm 1.21$  mill. km<sup>2</sup>. This is a reduction in SIA of 50% for the minimum summer month  
345 between the PI and LIG, but almost no change for the winter month MMM. Every model shows a reduction, often substantial,  
in summer sea ice between the PI and LIG. For the winter only one of the sixteen models show a (small) winter reduction in  
sea ice between the PI and LIG. This reinforces that the key seasons for understanding LIG warming are the spring, summer  
and autumn.

We investigate reasons for inter-model differences in LIG Arctic sea ice simulations: We find that the LIG total heat budget  
350 anomaly in the Arctic is due to (i) an increased downward SW flux in spring, resulting from the insolation forcing, and (ii)  
a decreased upward shortwave flux in summer, related to the decrease of the albedo due to the smaller sea-ice cover. During  
summer, this decrease in upward shortwave flux more than compensates the decrease in the SW down, which is maximum in  
August. Differences between the model results are due to a different phasing of the up and down SW anomalies in the different  
models, and are associated to the differences in model albedo.

355 Analysis of IPSLCM6 results shows differences in the properties of clouds, in terms of optical depth, between PI and LIG.  
Further work is required to identify if this is also important for other models. Changes in Arctic sea ice may also be related to  
ocean heat transport. Here, we have shown that ocean circulation changes occur for some, but not all, LIG simulations. Other  
factors which remain to be investigated include clouds and ocean heat uptake in the Arctic in the different models.

360 Most models agree with the reconstructed year round ice free northern North Atlantic. Model-data disagreement for the LIG  
occur over the Nordic Seas, close to Greenland and at the boundary with the Arctic Ocean, where many models overestimate  
annual mean sea ice concentration. This is not fully related to the model performance for summer. Indeed, 12 of 16 models

simulate little sea ice cover over the northernmost site and 10 of the models simulate less than 25% sea ice concentration over the site at 81.5°N . It is not possible, from the available data, to decide on best models, in particular in terms of summer sea ice. The northernmost site appears to discriminate those models which simulate very little sea ice at this site. However 365 models which do simulate > 75% summer sea ice concentration at this site also simulate >75% summer sea ice concentration for the two sites at 81.5 and 79.2°N , just South of the northernmost site, which is not realistic. More reconstructions with good chronology are needed in the Central Arctic to determine which model behaviour is more realistic, and in particular if the summer ice free Arctic simulated by the HadGEM3 model alone, among the 16 models, is possible. This would be key in 370 assessing ESMs used for future projections with respect to climates with much warmer summers than today. This is all the more crucial that there appear to be a nearly linear relationship between the ESM simulations of summer sea ice for the near future (years 50 to 70 of transient  $1\text{pctCO}_2$  simulations) and that simulated for the LIG: the models which responds strongly to the LIG forcing also respond strongly for the  $1\text{pctCO}_2$  forcing. This implies inter-comparisons between the LIG simulation, and simulations with moderate  $\text{CO}_2$  increase (during the transition to high  $\text{CO}_2$  levels), may yield insight into likely 21st century Arctic sea ice changes, especially if we achieve a more extensive characterisation of LIG Arctic sea ice from marine cores.

375 *Data availability.* The NOAA Optimum Interpolation (OI) V2 data set for sea ice concentration has been retrieved from <https://psl.noaa.gov/data/gridded/>. The data set used for the present study is the monthly data set: <ftp://ftp.cdc.noaa.gov/Datasets/noaa.oisst.v2/icec.mnmean.nc>.

The majority of the model simulations used in this study are available or will shortly be available on the Earth System Grid Federation (<https://esgf-node.llnl.gov/>), the data repository for CMIP6 simulations. The results of analyses from this original data, shown on Figures 2 to 12, will be referred to with a doi and accessible from the IPSL website upon acceptance of the manuscript.

380 *Author contributions.* MK, LS, MS, MG, and AdV(?) are joint first authors for this manuscript. MK and LS planned the study, with other QUIGs members. MK and MS analysed all model simulations and produced all model figures. LS wrote the manuscript. MG contributed substantially to the first draft and compiled all model information. AdV, IM, RS, and LS compiled the sea ice dataset, and IM produced the dataset map. DS co-planned some of the model analysis. MK, and all other here unnamed authors contributed model data. Ds, DF, CB, and JS provide sea ice modelling advice. All authors read the draft and commented on the text.

385 *Competing interests.* The authors declare that they have no competing financial interests

*Acknowledgements.* We acknowledge the QUIGS (Quaternary Interglacials working group endorsed by PAGES and PMIP) for making this comparison possible, in particular thanks to the workshop organised by this group in Cambridge, UK, in July 2019. We are grateful to the World Climate Research Programme, which, through its Working Group on Coupled Modelling, coordinated and promoted CMIP6. We thank the climate modeling groups for producing and making available their model output, the Earth System Grid Federation (ESGF) for

390 archiving the data and providing access, and the multiple funding agencies who support CMIP6 and ESGF. The Paleoclimate Modelling  
Intercomparison Project is thanked for coordinating the lig127k protocol and making the model-model and model-data comparisons possible  
within CMIP6. PMIP is endorsed by WCRP and CLIVAR. We also acknowledge NOAA/OAR/ESRL PSD, Boulder, Colorado, USA for their  
optimally interpolated sea-ice product, downloaded from their web site at <https://www.esrl.noaa.gov/psd/>. LS acknowledges support through  
395 NE/P013279/1, NE/P009271/1, and EU-TiPES. The project has received funding from the European Union's Horizon 2020 research and  
innovation programme under grant agreement No 820970. DS and MG acknowledges support from NERC research grant NE/P013279/1.  
MK is funded by CNRS and MS by a scholarship from CEA and "Convention des Services Climatiques" from IPSL (<https://cse.ipsl.fr/>).  
PM (Polina Morozova) was supported by the state assignment project 0148-2019-0009. EV (Evgeny Volodin) was supported by RSF grant  
20-17-00190. QZ acknowledges the HPC resources provided by the Swedish National Infrastructure for Computing (SNIC) at the National  
400 Supercomputer Centre (NSC). LM acknowledges support from the Australian Research Council FT180100606. BLO-B, and ECB acknowledge  
the CESM project, which is supported primarily by the National Science Foundation (NSF). This material is based upon work supported  
by the National Center for Atmospheric Research (NCAR), which is a major facility sponsored by the NSF under Cooperative Agreement  
No. 1852977. Computing and data storage resources, including the Cheyenne supercomputer (doi:10.5065/D6RX99HX), were provided by  
the Computational and Information Systems Laboratory (CISL) at NCAR.

Table 1: Marine core records of Arctic sea ice from MISSe. The references indicated for the dinocyst reconstructions are those for the initial core, the reconstruction itself follows de Vernal et al. (2013a, b, 2019) (c.f. main text for details). SIC stands for 'sea ice concentration'.

Latitude (°N)	Longitude (°E)	Sea-ice indicator	Core name	Reference	Site # on map	Chronol. control	Qualitative sea-ice state	Duration of SIC > 0.50, in months / year			Annual mean SIC		
								1=Good	2=Uncertain	Min	Max	Min	Max
87.08	144.77	Ostracode faunas	Oden96/12-1pc	Cronin et al. (2010)			Perennial sea ice (summer sea ice concentration >75%)	?	?	?	?	?	?
85.32	-14	IP25/PIP25	PS2200-5	Stein et al. (2017)			Perennial sea ice (summer sea ice concentration >75%)	?	?	?	?	?	?
85.32	-14	Ostracode faunas	PS2200-5	Cronin et al. (2010)			Perennial sea ice (summer sea ice concentration >75%)	?	?	?	?	?	?
85.14	-171.43	IP25/PIP25	PS51/38-3	Stein et al. (2017)			Perennial sea ice	?	?	?	?	?	?
84.81	-74.26	Subpolar foraminifers	GreenICE (core 11)	Nørgaard- Pedersen et al. (2007)			Reduced sea ice cover, partly even seasonally ice-free? (but: regional signal or just local polynya conditions?)	?	?	?	?	?	?
81.92	13.83	IP25/PIP25	PS92/039-2	Kremser et al. (2018b)			Perennial sea ice (summer sea ice concentration >75%)	?	?	?	?	?	?
81.54	30.17	Dinocysts	PS2138-1	Matthiessen and Knieß (2001)			Seasonal sea-ice conditions summer probably ice-free	0	5	0	0	0.3	0.3
81.54	30.59	IP25/PIP25	PS2138-1	Stein et al. (2017)			Seasonal sea-ice conditions summer probably ice-free	?	?	?	0.1	0.1	0.3

81.19	140.04	IP25/PIP25	PS2757-8	Stein et al. (2017)	4	2	Perennial sea ice	?	?	?	?	
79.59	-172.50	Subpolar foraminifers	HLY0503- 8IPC	Adler et al. (2009)	3	2	Seasonal sea-ice conditions summer probably ice-free	?	?	?	?	
79.32	-178.07	Ostracode faunas	NP26-32	Cronin et al. (2010)	1	2	Perennial sea ice (summer sea ice concentration >75%)	?	?	?	?	
79.20	4.67	IP25/PIP25	PS93/006-1	Kremmer et al. (2018a)	11	1	Seasonal sea-ice conditions summer probably ice-free	?	?	0.3	0.6	
78.98	-178.15	Ostracode faunas	NP26-5	Cronin et al. (2010)	2	2	Perennial sea ice (summer sea ice concentration >75%)	?	?	?	?	
76.85	8.36	Dinocysts	M23455-3	Nieuwenhove et al. (2011)	Van	12	1	Nearly ice free all year round	0	1	0	0.15
70.01	-12.43	Dinocysts	M23352	Nieuwenhove et al. (2013)	N. Van	13	1	Nearly ice free all year round	0	1	0	0.15
69.49	-17.12	Dinocysts	PS1247	N. Van et al. (2011)	Nieuwenhove et al. (2013)	14	1	Nearly ice free all year round	0	2	0	0.2
67.77	5.92	Dinocysts	M23323	Nieuwenhove et al. (2011)	Van	15	1	Nearly ice free all year round	0	1	0	0.15
60.58	-22.07	Dinocysts	MD95-2014	Eynaud (1999)	17	1	Ice free all year round	0	0	0	0	

58.77	-25.95	Dinocysts	MD95-2015	Eynaud et al. (2004)	18	1	all year round	0	0	0	0
58.21	-48.37	Dinocysts	HU90-013-13P	Hillaire-Marcel et al. (2001); de Vernal and Hillaire-Marcel (2008)	19	1	Nearly ice free all year round	0	1	0	0.15
55.47	-14.67	Dinocysts	MD95-2004	Nieuwenhove et al. (2011)	20	1	all year round	0	0	0	0
53.33	-45.26	Dinocysts	HU91-045-91	This manuscript	21	1	all year round	0	1	0	0.15
53.06	-33.53	Dinocysts	IODP1304	This manuscript, Hodell et al. 2009 for the chronology	22	1	Nearly ice free all year round	0	1	0	0.15
50.17	-45.63	Dinocysts	IODP1302/1303	This manuscript, Hillaire-Marcel et al. 2011 for the chronology	23	1	Nearly ice free all year round	0	1	0	0.15
46.83	-9.52	Dinocysts	MD03-2692	Penaud et al. (2008)	24	1	all year round	0	0	0	0.15
37.80	-10.17	Dinocysts	MD95-2042	Eynaud et al. (2000)	25	1	all year round	0	0	0	0

**Table 2:** Overview of models that have run the CMIP6-PMIP4 LIG simulation. For each model, denomination, physical core components, horizontal and vertical grid specifications, details on prescribed vs interactive boundary conditions, reference publication and LIG simulation length is shown.

Model name (abbreviation)	Physical core components	Model grid (i_lon X i_lat X z_lev)	Boundary Conditions	Reference publication	LIG simulation length (yrs)
<b>ACCESS-ESM1-5</b> (ACCESS)	Atmosphere: UM Land: CABLE2.4 Ocean: MOM5 Sea Ice: CICE4.1	Atmosphere: 192x145 x L38 Ocean: 360x300 x L50	Vegetation: prescribed Aerosol: prescribed Ice-Sheet: prescribed	Ziehn et al. (2017)	Spin-up: 400 Production: 200
<b>AWIESM-1-1-LR</b> (AWIESM1)	Atmosphere: ECHAM6.3.04p1 Land: JSBACH 3.20 Ocean: FESOM 1.4 Sea Ice: FESOM 1.4	Atmosphere: 192x96 x L47 Ocean: unstructured grid 126859 nodes x L46	Vegetation: Interactive Aerosol: prescribed PI Ice-Sheet: prescribed	Sidorenko et al. (2015)	Spin-up: 1000 Production: 100
<b>AWIESM-2-1-LR</b> (AWIESM2)	Atmosphere: ECHAM6.3.04p1 Land: JSBACH 3.20 Ocean: FESOM 2 Sea Ice: FESOM 2	Atmosphere: 192x96 x L47 Ocean: unstructured grid 126858 nodes x L48	Vegetation: interactive Aerosol: prescribed Ice-Sheet: prescribed	Sidorenko et al. (2019, 2015)	Spin-up: 1000 Production: 100
<b>CESM2</b>	Atmosphere: CAM6 Land: CLM5 Ocean: POP2 Sea Ice: CICE5.1	Atmosphere: 288x192 x L32 Ocean: 320x384 x L60	Vegetation: prescribed Aerosol: interactive Ice-Sheet:	Danabasoglu et al. (2019)	Spin-up: 325 Production: 700
<b>CNRM-CM6-1</b> (CNRM-CM6)	Atmosphere: ARPEGE-Climat Land: ISBA-CTRP Ocean: NEMO3.6 Sea Ice: GELATO6	Atmosphere: 256x128 x L91 (Triangular-Linear 127) Ocean: 362x294 x L75	Vegetation: prescribed Aerosol: prescribed PI Ice-Sheet: prescribed	Volodire et al. (2019)	Spin-up: 100 Production: 200
<b>EC-Earth3</b> (EC-Earth)	Atmosphere: IFS-cy36r4 Land: HTESSEL Ocean: NEMO3.6 Sea Ice: LIM3	Atmosphere: T159(480x240)xL62 Ocean: 362x292 x L75	Vegetation: prescribed Aerosol: prescribed Ice-Sheet: prescribed	Hazeleger et al. (2012)	Spin-up: 300 Production: 200

<b>GISS-E2.1-G</b>	Atmosphere: GISS-E2.1	Atmosphere: 2x2.5 x 40L	Vegetation: Ent / NotDynamic	Kelley et al.	Spin-up: 1000 yrs Production: 100
	Land: GISS-E2.1 Ocean: GISS Sea Ice: GISS	Ocean: 1x1.25 x 40L	Aerosol: NINT Ice-Sheet: N/A		
<b>HadGEM3-GC3.1-LL</b> (HadGEM3)	Atmosphere: MetUM-GA7.1 Land: JULES-GA7.1 Ocean: NEMO-GO6.0 Sea Ice: CICE-GSI8	Atmosphere: 192x144 x L85 Ocean: 360x330 x L75	Vegetation: prescribed Aerosol: Prescribed Ice-Sheet: prescribed	Williams et al. (2018)	Spin-up: 350 Production: 200
	Atmosphere: INM-AM4-8 Land: INM-LND1 Ocean: INM-OM5 Sea Ice: INM-ICE1	Atmosphere: 180x120 x L21 Ocean: 360x318 x L40	Vegetation: prescribed Aerosol: interactive Ice-Sheet: prescribed		
<b>INM-CM4-8</b>	Atmosphere: LMDZ6 Land: ORCHIDEE Ocean: NEMO-OPA Sea Ice: NEMO-LIM3	Atmosphere: 144x143 x L79 Ocean: 362x332 x L75	Vegetation: prescribed PFTs, interactive phenology Aerosol: Prescribed PI values Ice-Sheet: prescribed	Volodin et al. (2018)	Spin-up: 50 Production: 100
	Atmosphere: ECBilt Land: VECODE Ocean: CLIO	Atmosphere: 64x32 x L3 Ocean: 120x65 x L20	Vegetation: interactive Aerosol: - Ice-Sheet: prescribed		
<b>IPSL-CM6A-LR</b>	Atmosphere: CCSR AGCM Land: MATSIRO6.0 +VISIT-e Ocean: COCO4.9 Sea Ice: COCO4.9	Atmosphere: 128x64 x L40 Ocean: 360x256 x L63	Vegetation: prescribed Aerosol: prescribed Ice-Sheet: prescribed	Boucher et al. (2019)	Spin-up: 300 Production: 200
	Atmosphere: ECHAM6.3 Land: JS-BACH Ocean: NEMO3.4 Sea Ice: CICE4.1	Atmosphere: 192x96 x L47 Ocean: 384x362 x L46	Vegetation: interactive Aerosol: prescribed Ice-Sheet: prescribed		
<b>LOVECLIM1.2</b>	Atmosphere: CAM4 Land: CLM4 Ocean: MICOM Sea Ice: CICE4	Atmosphere: 144x96 x L26 Ocean: 360x384 x L53	Vegetation: prescribed, as PI Aerosol: prescribed, as PI Ice-Sheet: prescribed, as PI	Goosse et al. (2010)	Spin-up: 3000 Production: 1000
	Atmosphere: CCSR AGCM Land: MATSIRO6.0 +VISIT-e Ocean: COCO4.9 Sea Ice: COCO4.9	Atmosphere: 128x64 x L40 Ocean: 360x256 x L63	Vegetation: prescribed Aerosol: prescribed Ice-Sheet: prescribed		
<b>MIROC-ES2L</b>	Atmosphere: ECHAM6.3 Land: JS-BACH Ocean: NEMO3.4 Sea Ice: CICE4.1	Atmosphere: 192x96 x L47 Ocean: 384x362 x L46	Vegetation: interactive Aerosol: prescribed Ice-Sheet: prescribed	Hajima et al. (2019) Tatebe et al. (2018)	Spin-up: 1450 Production: 100
	Atmosphere: CAM4 Land: CLM4 Ocean: MICOM Sea Ice: CICE4	Atmosphere: 144x96 x L26 Ocean: 360x384 x L53	Vegetation: prescribed, as PI Aerosol: prescribed, as PI Ice-Sheet: prescribed, as PI		
<b>NESM3</b>	Atmosphere: GISS-E2.1	Atmosphere: 2x2.5 x 40L	Vegetation: Ent / NotDynamic	Cao et al. (2018)	Spin-up: 500 Production: 100
	Land: GISS-E2.1 Ocean: GISS Sea Ice: GISS	Ocean: 1x1.25 x 40L	Aerosol: NINT Ice-Sheet: N/A		
<b>NorESM1-F</b> (NORESM1)	Atmosphere: MetUM-GA7.1 Land: JULES-GA7.1 Ocean: NEMO-GO6.0 Sea Ice: CICE8	Atmosphere: 192x144 x L85 Ocean: 360x330 x L75	Vegetation: prescribed Aerosol: Prescribed Ice-Sheet: prescribed	Guo et al. (2019)	Spin-up: 500 Production: 200
	Atmosphere: INM-AM4-8 Land: INM-LND1 Ocean: INM-OM5 Sea Ice: INM-ICE1	Atmosphere: 180x120 x L21 Ocean: 360x318 x L40	Vegetation: prescribed Aerosol: interactive Ice-Sheet: prescribed		

<b>NorESM2-LM (NORESM2)</b>	Atmosphere: CAM-OSLO	Atmosphere: Land: CLM Ocean: BLOM Sea Ice: CICE	144x96 x L32 Ocean: 360x384 x L53	Vegetation: as in PI Aerosol: as in PI Ice-Sheet: as in PI	Seland et al. (2019)	Spin-up: 300 Production: 200

**Table 3.** Astronomical parameters and atmospheric trace gas concentrations used to force LIG and PI simulations.

<b>Astronomical parameters</b>	<b>LIG</b>	<b>PI</b>
Eccentricity	0.039378	0.016764
Obliquity	24.040°	23.459°
Perihelion-180°	275.41°	100.33°
Date of vernal equinox	March 21 at noon	March 21 at noon
<b>Trace gases</b>		
CO2	275 ppm	284.3 ppm
CH4	685 ppb	808.2 ppb
N2O	255 ppb	273 ppb

**Table 4.** Sea ice area and extent (in  $10^6$  km $^2$ ) for the PI and LIG simulations. MMM stands for the multi-model mean, STD for the multi-model standard deviation.

Model or dataset	PI sea ice area		LIG sea ice area		PI sea ice extent		LIG sea ice extent	
	minimum (month)	maximum (month)	minimum (month)	maximum (month)	minimum (month)	maximum (month)	minimum (month)	maximum (month)
NOAA_OI_v2	5.65 (8)	14.44 (2)	na	na	7.73 (8)	17.05 (2)	na	na
ACCESS	5.49 (8)	14.90 (2)	2.05 (8)	14.01 (2)	7.93 (8)	17.04 (2)	4.44 (8)	15.85 (2)
AWIESM1	5.39 (8)	15.59 (2)	3.58 (8)	17.53 (2)	8.52 (8)	18.42 (2)	6.88 (8)	20.82 (2)
AWIESM2	5.19 (8)	11.89 (2)	3.14 (8)	12.28 (2)	7.78 (8)	13.90 (2)	5.92 (8)	14.87 (2)
CESM2	5.45 (8)	14.12 (2)	1.18 (8)	14.53 (2)	7.92 (8)	15.26 (2)	2.55 (8)	15.81 (2)
CNRM-CM6-1	6.07 (8)	16.02 (2)	4.29 (8)	16.94 (2)	8.44 (8)	18.32 (2)	6.41 (8)	19.62 (2)
EC-Earth	7.49 (7)	15.89 (2)	3.46 (7)	13.93 (2)	10.13 (7)	18.46 (2)	6.01 (8)	16.16 (2)
FGOALS-g3	8.54 (7)	17.46 (1)	5.04 (8)	19.51 (2)	11.40 (7)	20.20 (1)	7.78 (8)	22.14 (2)
GISS-E2-1-G	8.70 (8)	17.08 (2)	5.41 (8)	17.49 (2)	11.13 (8)	21.58 (2)	7.83 (8)	22.20 (2)
HadGEM3	5.40 (7)	13.40 (2)	0.23 (8)	14.50 (2)	7.58 (7)	15.20 (2)	0.07 (8)	16.52 (2)
INMCM4-8	7.88 (7)	17.24 (2)	5.71 (8)	17.14 (2)	10.47 (7)	20.99 (2)	8.24 (8)	20.83 (2)
IPSLCM6	6.39 (7)	16.91 (2)	2.46 (8)	17.82 (2)	8.88 (7)	19.91 (2)	4.24 (8)	21.02 (2)
LOVECLIM	8.64 (7)	14.56 (1)	3.06 (7)	16.66 (2)	10.90 (7)	16.52 (1)	6.96 (7)	18.85 (1)
MIROC-ES2L	4.27 (7)	13.17 (2)	3.05 (7)	13.49 (2)	7.04 (7)	14.87 (2)	4.98 (8)	15.19 (2)
NESM3	5.20 (8)	18.50 (2)	1.28 (8)	22.39 (2)	7.67 (8)	20.80 (2)	2.96 (8)	24.50 (2)
NORESM1	5.03 (8)	12.64 (1)	2.31 (8)	13.11 (2)	7.30 (8)	14.00 (1)	4.52 (8)	14.62 (2)
NORESM2	5.62 (8)	13.38 (1)	2.22 (8)	13.89 (2)	8.02 (8)	14.66 (1)	4.26 (8)	15.12 (2)
MMM	6.46 (7)	15.16 (2)	3.20 (8)	15.95 (2)	8.89 (7)	17.48 (2)	5.39 (8)	18.38 (2)
STD	1.41	1.90	1.50	2.61	1.41	1.90	2.13	3.12

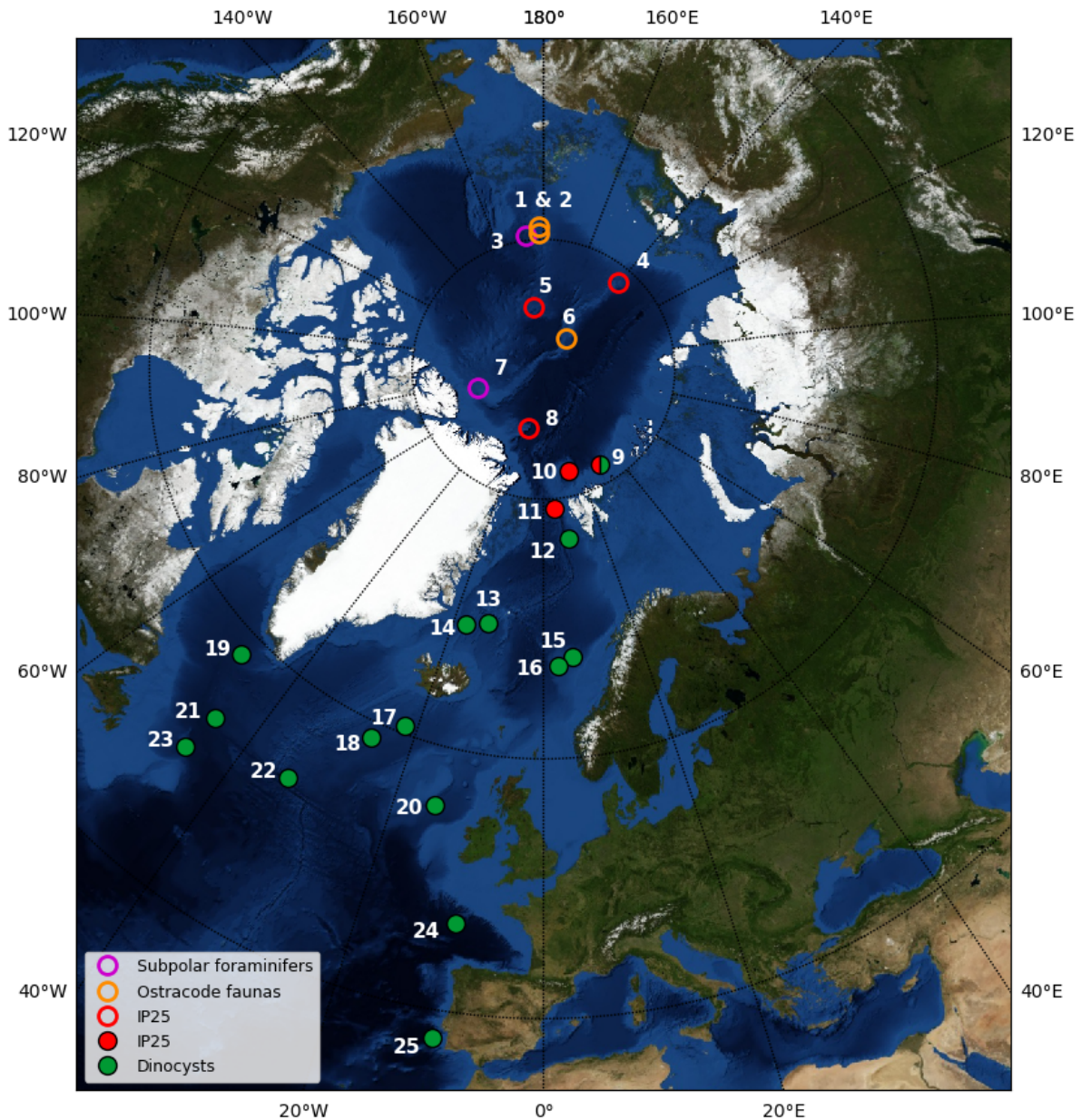


**Figure 1.** Map showing the location of the LIG Arctic sediment cores listed in Table 1. Open symbols correspond to records with uncertain chronology, filled symbols to records with good chronology. The map background has been created using <http://visibleearth.nasa.gov>.

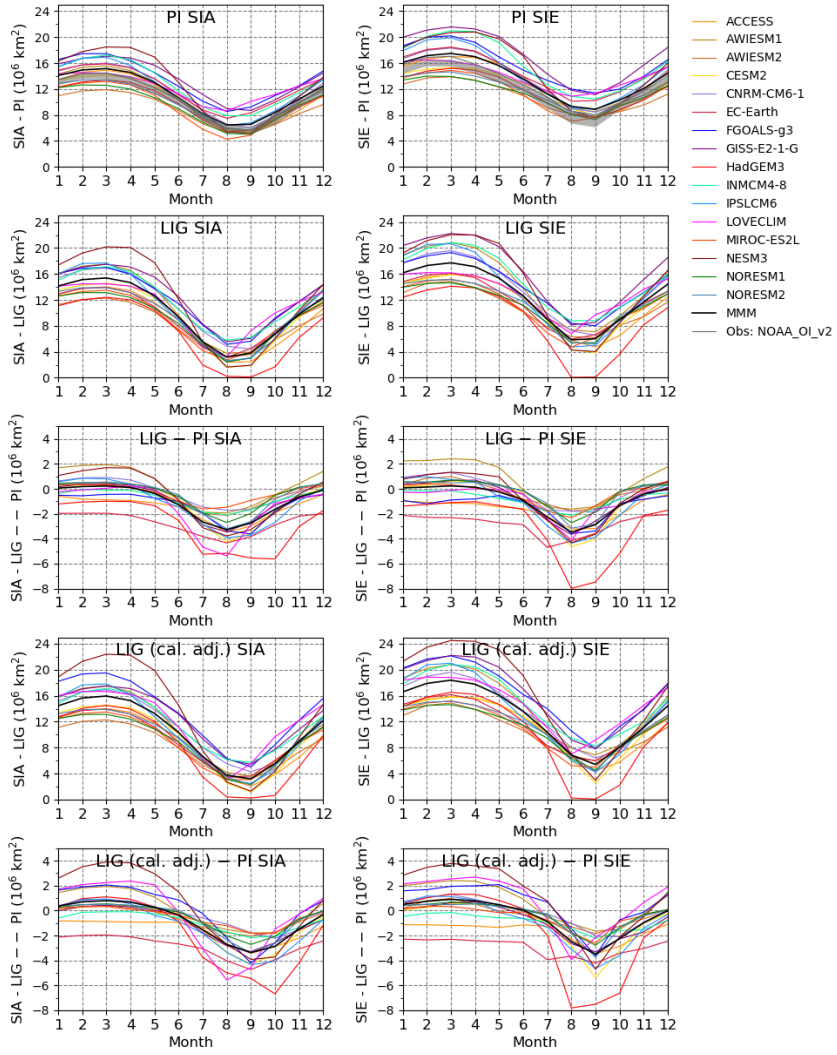


**Figure 2.** Mean seasonal cycle of the Arctic sea-ice area (SIA, l.h.s.) and sea ice extent (SIE, r.h.s.), in  $10^6 \text{ km}^2$ , simulated for the PI and LIG periods by the PMIP4 models. The top row show the results for PI. The grey shading shows the the monthly minimum/maximum in the SIA and SIE observed over the years 1982–2001, as given by the NOAA\_OI\_v2 data set. The 2nd and 4th row show the LIG results, with no calendar adjustment (2nd row) and with calendar adjustment (4th row). The 3rd and bottom row show the corresponding LIG – PI anomalies, with no calendar adjustment (3rd row) and with calendar adjustment (bottom row).

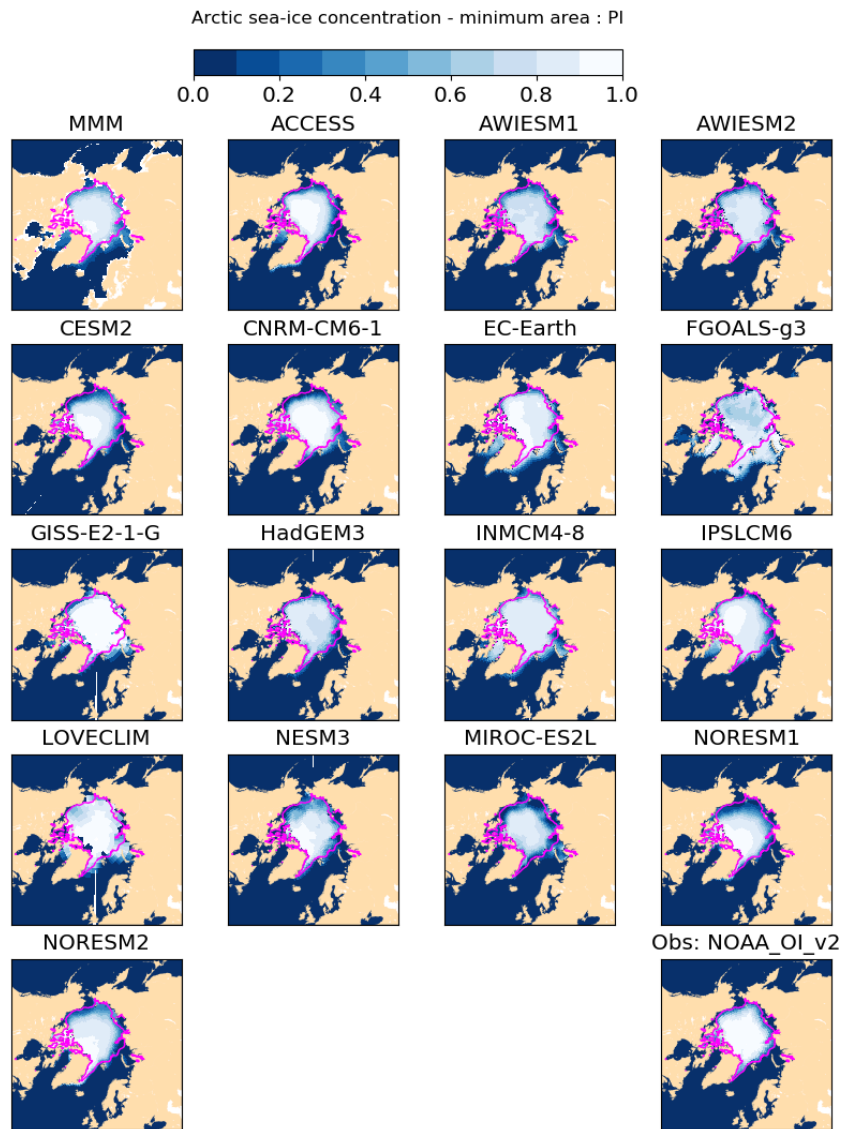


**Figure 3.** PI sea-ice concentration for the month of minimum SIA as computed for Figure 2. The magenta contour shows the 0.15 isocontour of the NOAA\_OI\_v2 observations (Reynolds et al., 2002, cf. *Data availability* section) averaged over years 1982–2001.

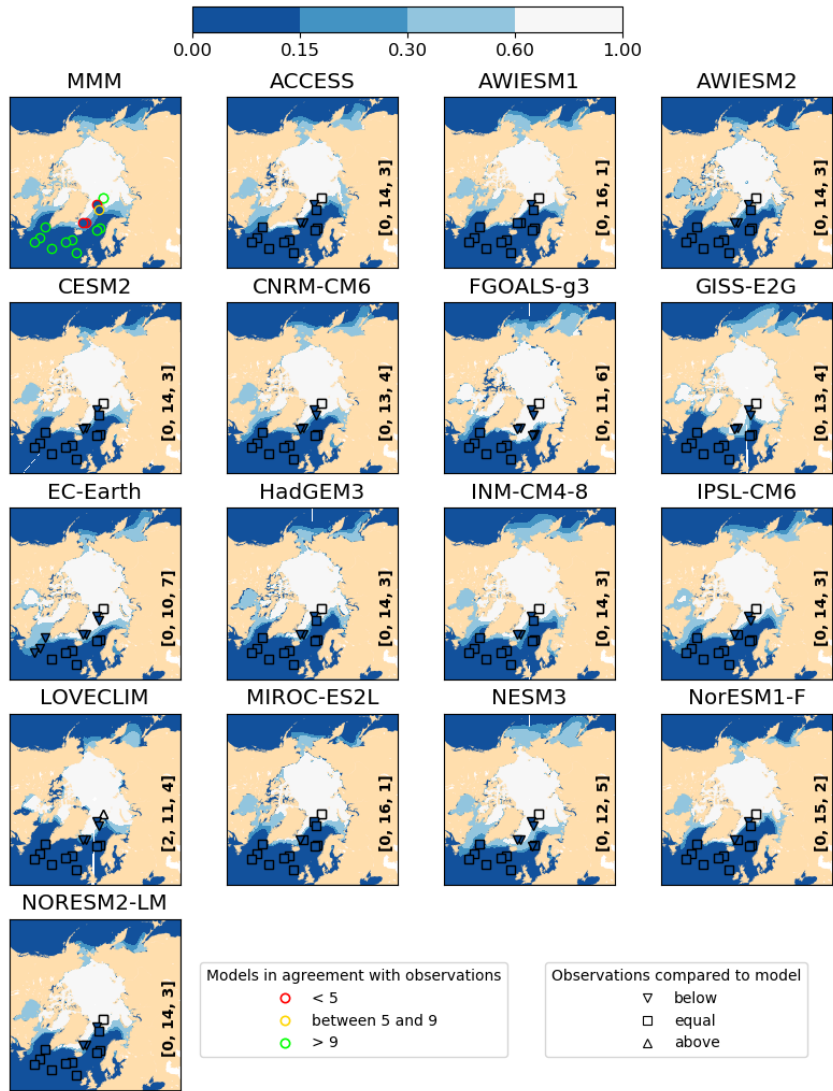


**Figure 4.** Sea ice annual concentration simulated for PI, for the multi-model mean (MMM) and for each model. The color filling of the symbols on the maps correspond to the observed values at each site, according to the NOAA\_OI\_v2 data set, classified into 3 categories: perennial cover (9 to 12 months), seasonal cover (3 to 9 months), ice free state (0 to 3 months). On the MMM panel, for each data site, the color of the symbol outline corresponds to the number of models simulating the observed ice cover. On the panels for individual models, the shape of the symbol depends on the model result being below the observed one (triangle down), above the observed one (triangle up) or in the same category as the observed one (circle). The number of data points which are above, equal and below the number of months simulated by models are written at the bottom right corner of each panel.

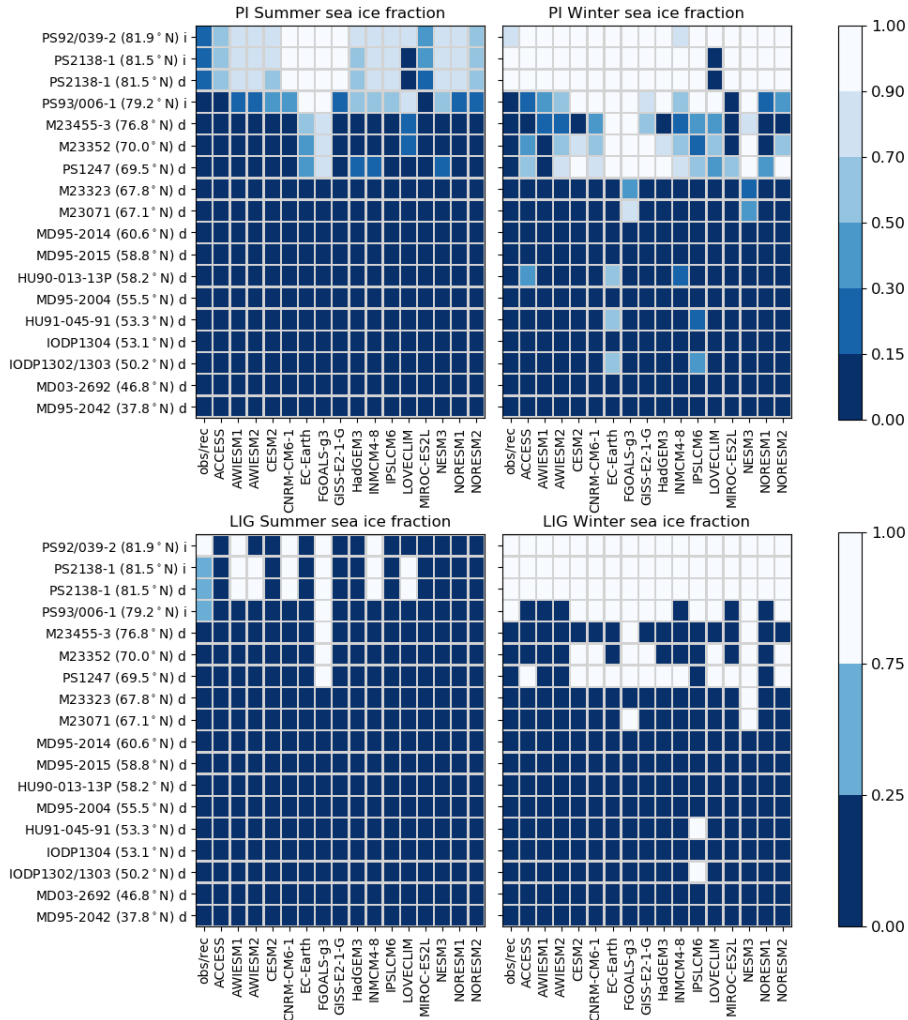


**Figure 5.** Model-data comparison as a function of latitude and record site for PI (top row) and LIG (bottom row). For each LIG data site, the NOAA\_OI\_v2 observations (PI) or reconstructions (LIG) are shown in the first column of each plot, and the model results in the columns to the right. For PI, both the model results and the data are shown in terms of sea ice fraction averaged over the month of minimum (l.h.s) or maximum (r.h.s) northern hemisphere sea ice area and the previous and following months. For the LIG, the qualitative assessments (eighth columns of Table 1 have been used, for records with good chronological control. The letter next to the name of the site stands for indicator used for the reconstruction: dinocysts ("d") or IP25/PIP25 ("i"). For summer conditions, dark blue shading is used for the "no sea ice" category, light blue shading for "summer probably ice free" conditions, and white shading for "summer sea ice concentration > 75%" and "Perennial sea ice". For winter, dark blue shading is used for "ice free all year round" conditions and white shading for "Seasonal sea-ice conditions" and "Perennial sea-ice". The model results are averaged like for PI, and shown following the colour scale to the r.h.s. of the plots.

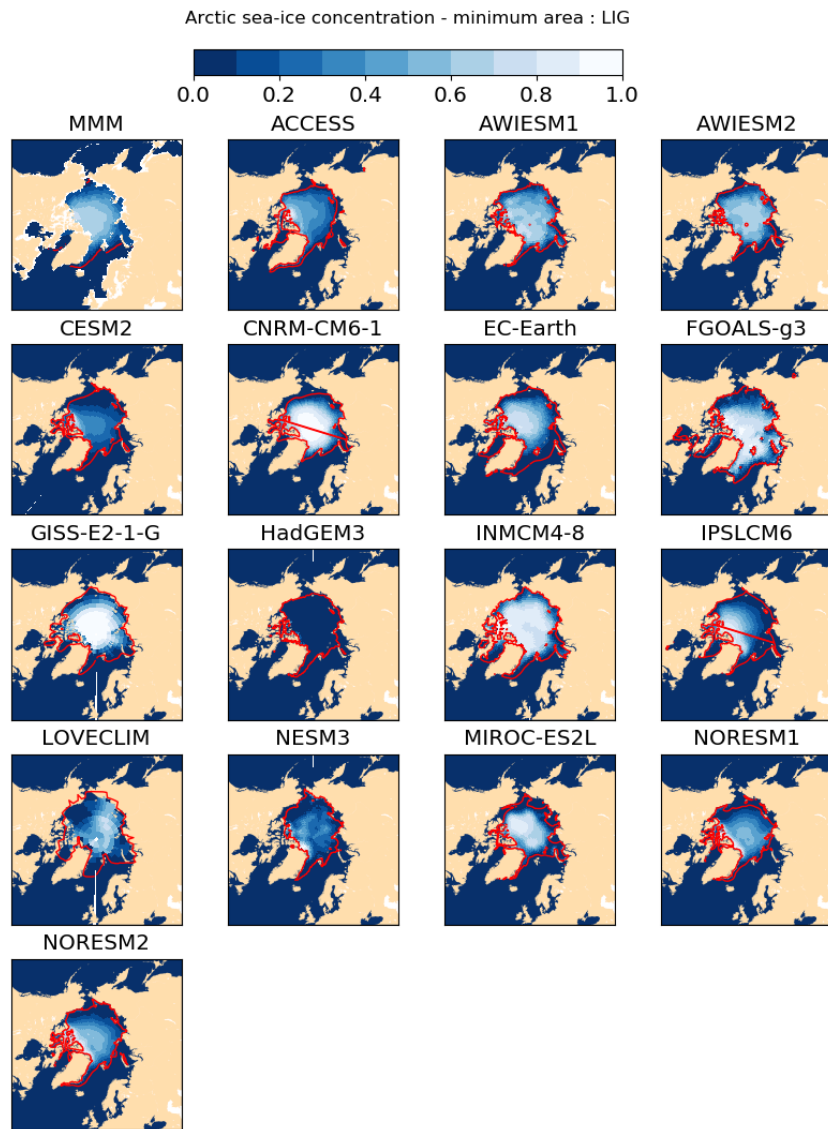


**Figure 6.** LIG sea-ice concentration for the month of minimum SIA (computed with calendar adjustment) as computed for Figure 2. The magenta contour shows the 0.15 isocontour of the corresponding PI simulation.

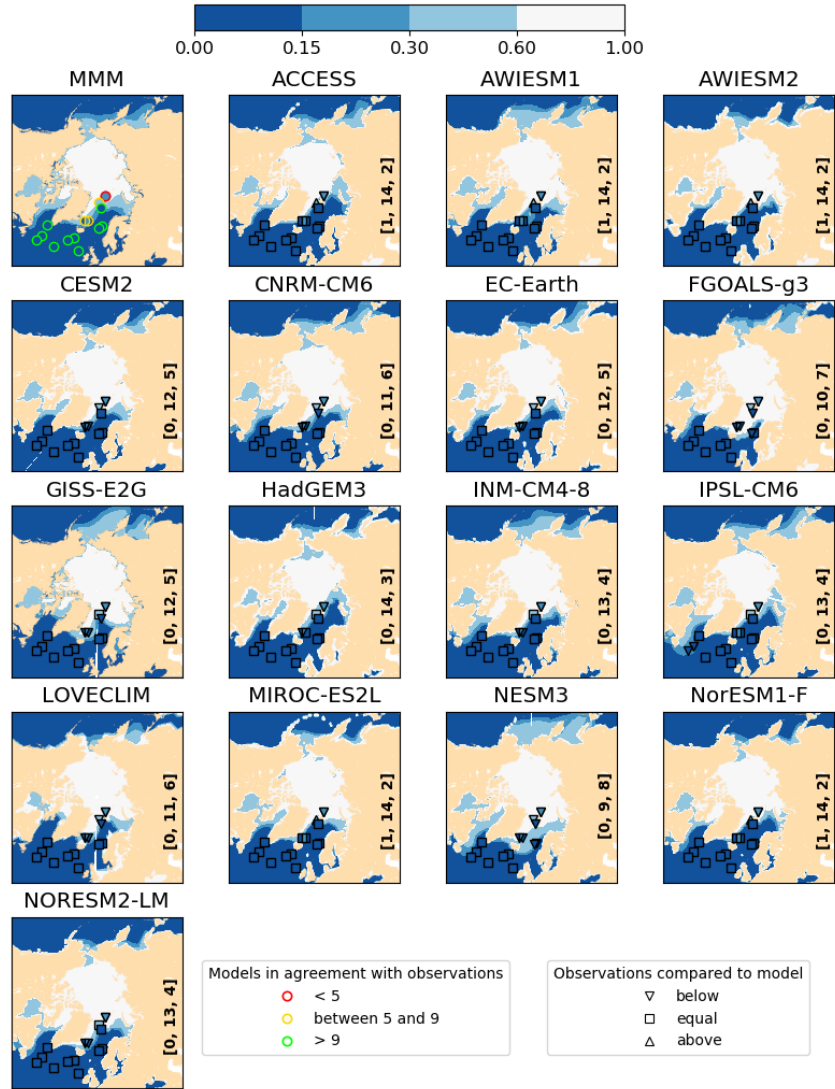


**Figure 7.** Sea ice annual concentration during the LIG, for the multi-model mean (MMM) and for each model. The color filling of the symbols on the maps correspond to the reconstructed values, classified into 3 categories: perennial cover (9 to 12 months), seasonal cover (3 to 9 months), ice free state (0 to 3 months). On the MMM panel, for each data site, the color of the symbol outline corresponds to the number of models simulating the reconstructed ice cover. On the panels for individual models, the shape of the symbol depends on the model result being below the reconstructed one (triangle down), above the reconstructed one (triangle up) or in the same category as the reconstructed one (circle). The number of data points which are above, equal and below the number of months simulated by models are written at the bottom right corner of each panel.

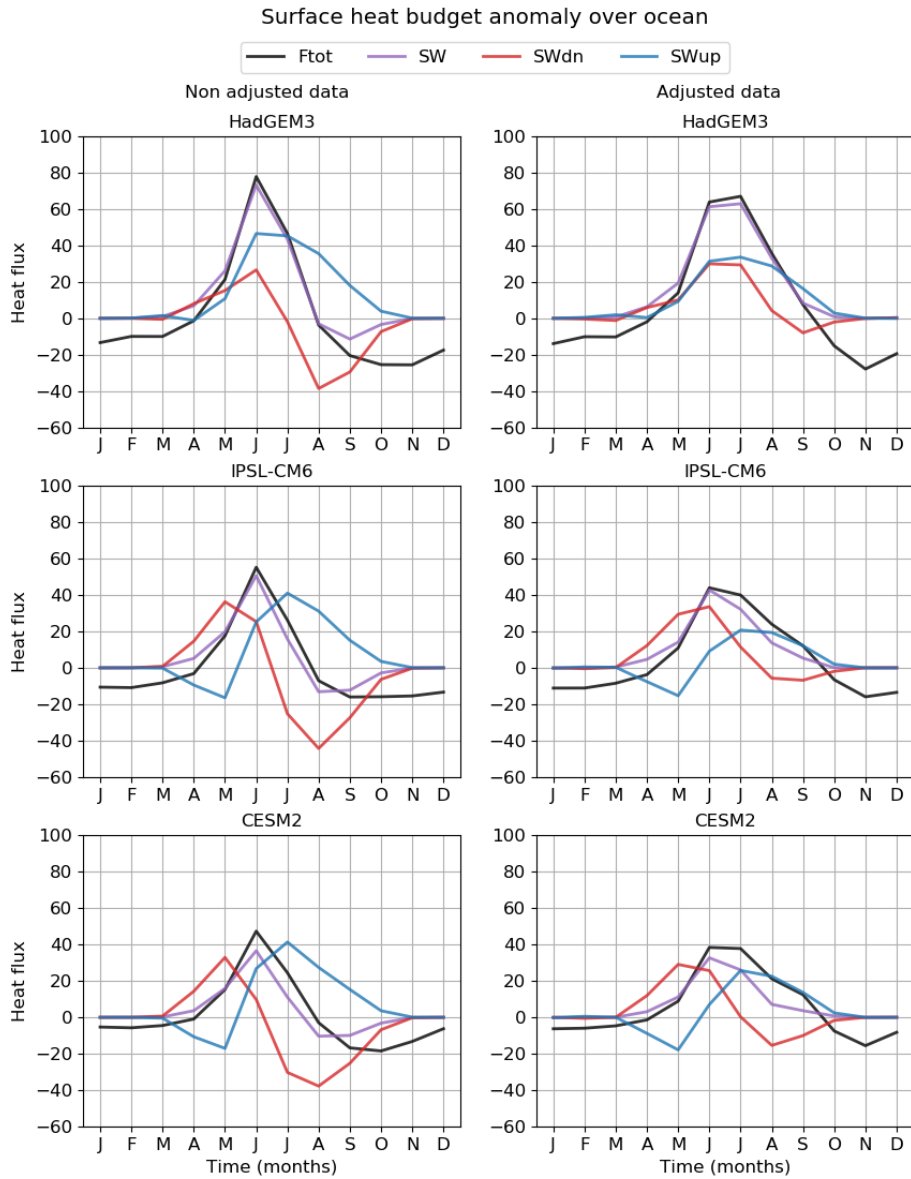


**Figure 8.** Main components of the atmospheric energy budget averaged over the Arctic ( $70\text{--}90^{\circ}\text{N}$ ) for HadGEM3, CESM2 and IPSLCM6. The LIG-PI anomalies as shown as a function of the month for the total energy budget (Ftot, black), the SW budget (SW, violet), and for the downward (SWdn, red) and upward SW (SWup, blue) fluxes, all counted positive downward. The r.h.s column shows results for which the LIG calendar has been taken into account (for the LIG simulations) while the l.h.s. column shows the results averaged on the PI calendar both for PI and LIG.

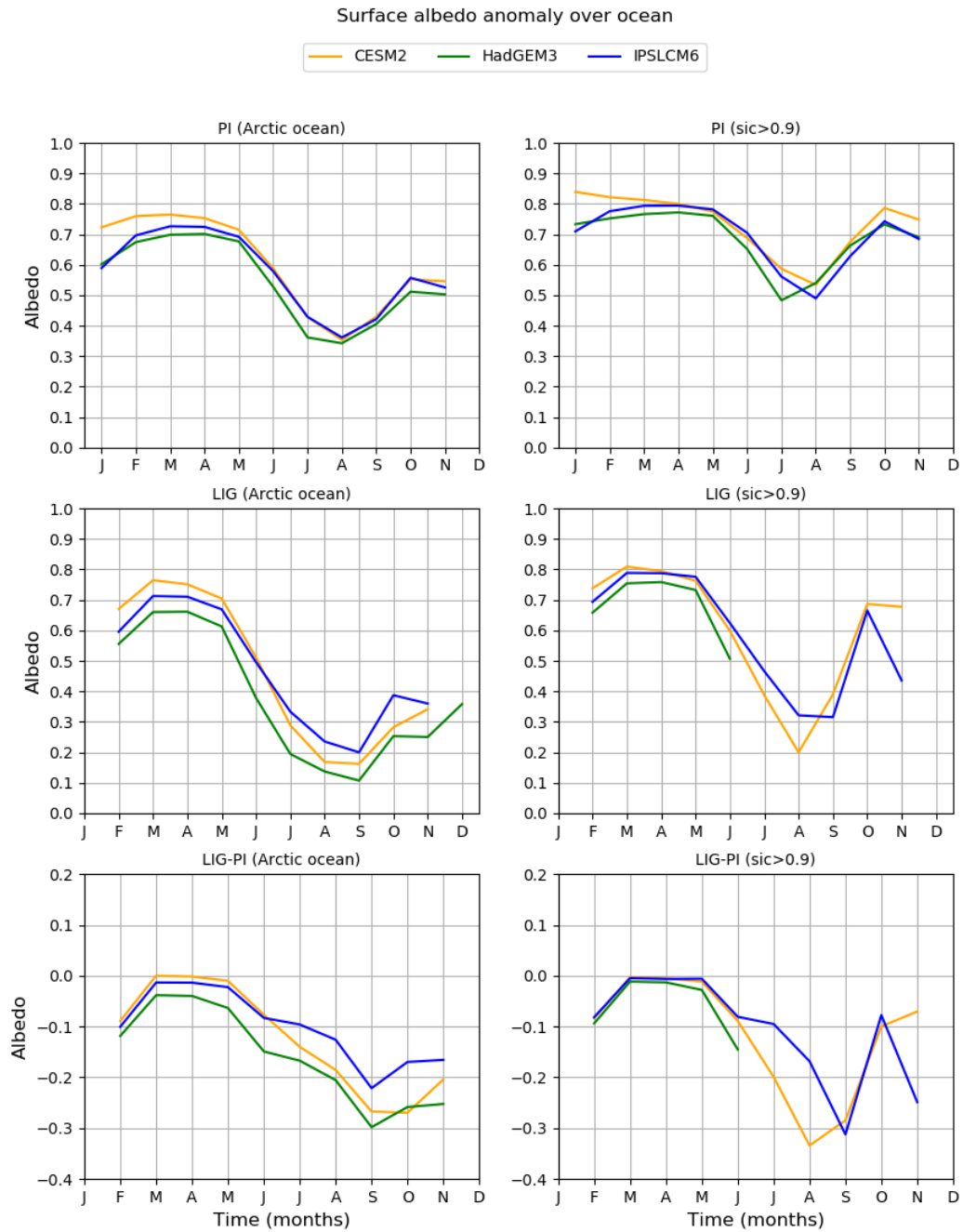


**Figure 9.** Albedo over the Arctic for PI (top), LIG (middle) and LIG-PI (bottom) for HadGEM3, IPSL-CM6 and CESM2. The albedo has been recomputed from the SWup and SWdn fluxes. The l.h.s. column shows the results for the whole Arctic, while the r.h.s. column shows the results for areas where the sea ice fraction is larger than 0.9.

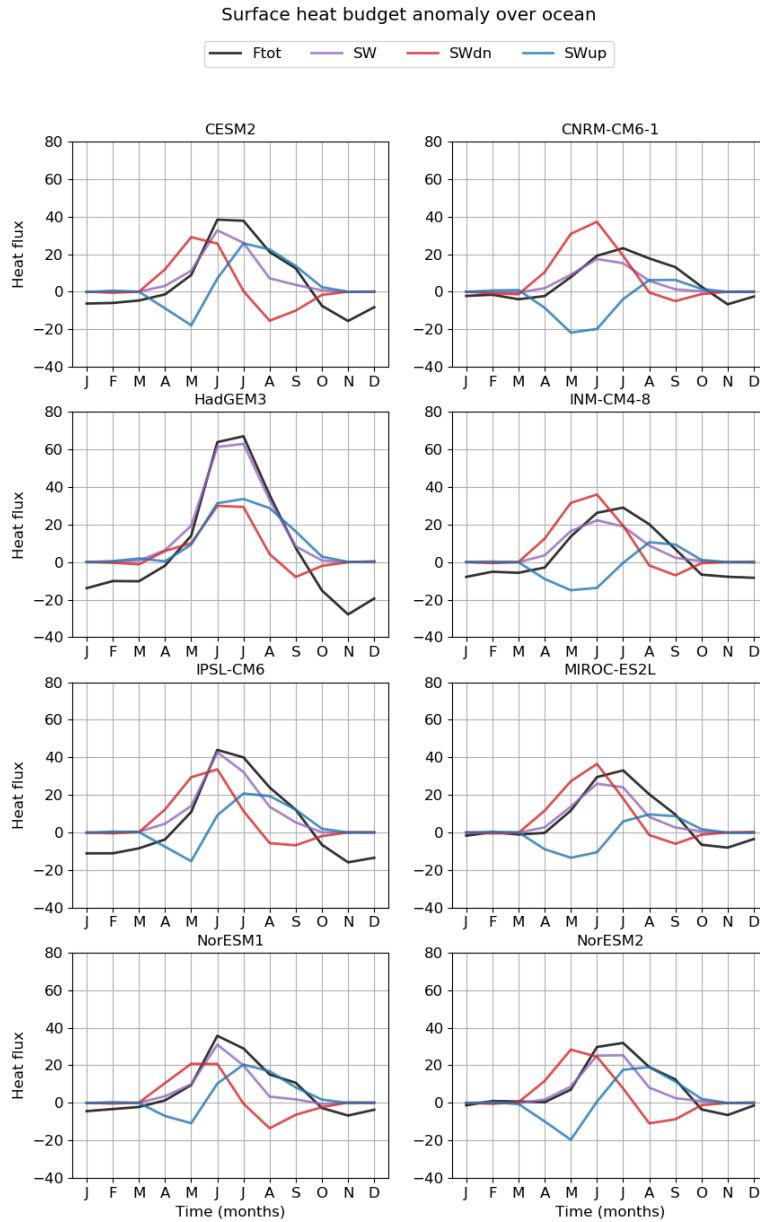


**Figure 10.** Main components of the atmospheric energy budget averaged over the Arctic ( $70\text{--}90^\circ\text{N}$ ) for HadGEM3, CESM2, CNRM-CM6-1, IPSLCM6, INM-CM4-8, MIROC-ES2L, NorESM1, NorESM2. The LIG-PI anomalies as shown as a function of the month for the total energy budget (black), the SW budget (violet), and for the downward (red) and upward SW (blue) fluxes, all counted positive downward.

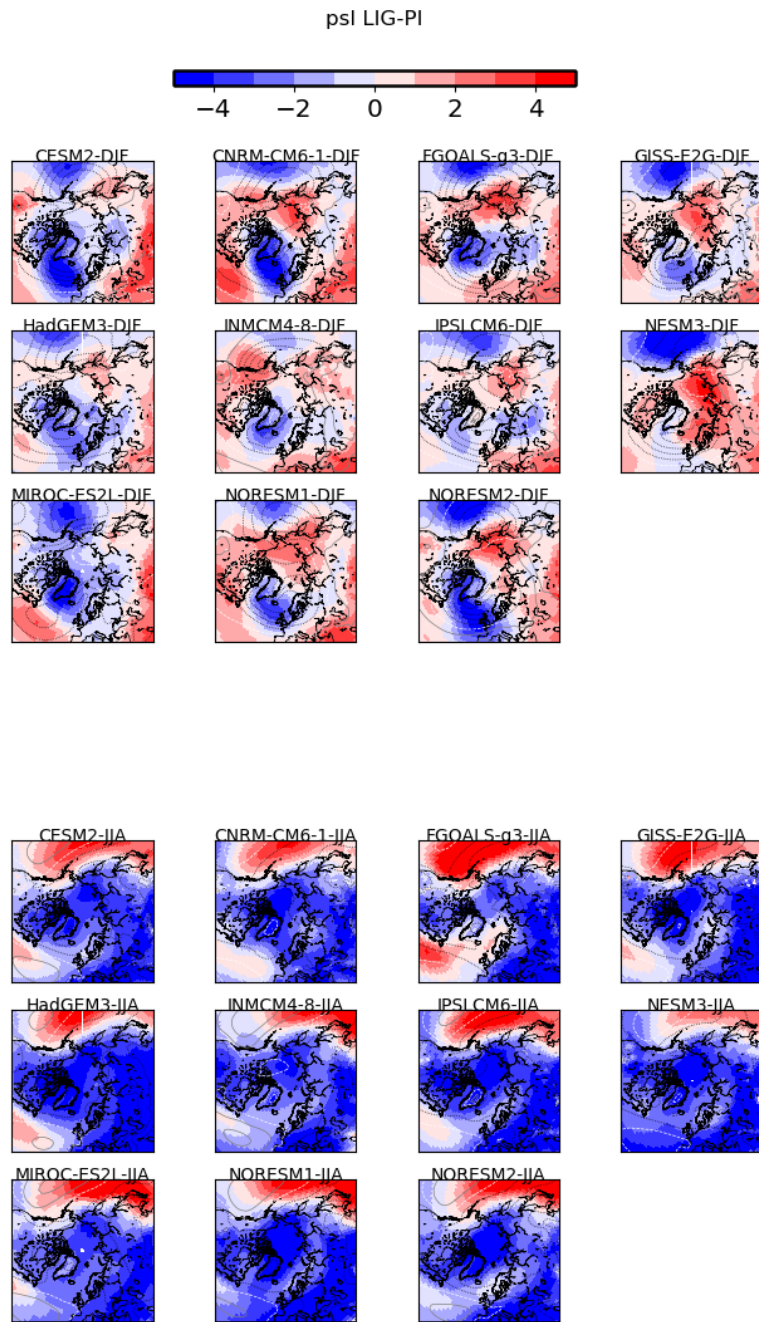


**Figure 11.** Anomalies (LIG – PI, hPa, shading) in mean sea level pressure for DJF (top plots) and JJA (bottom plots). Contours indicating PI values are superimposed: values every 5 hPa, 1005 hPa isobar in white, black contours for lower values, grey contours for higher values.

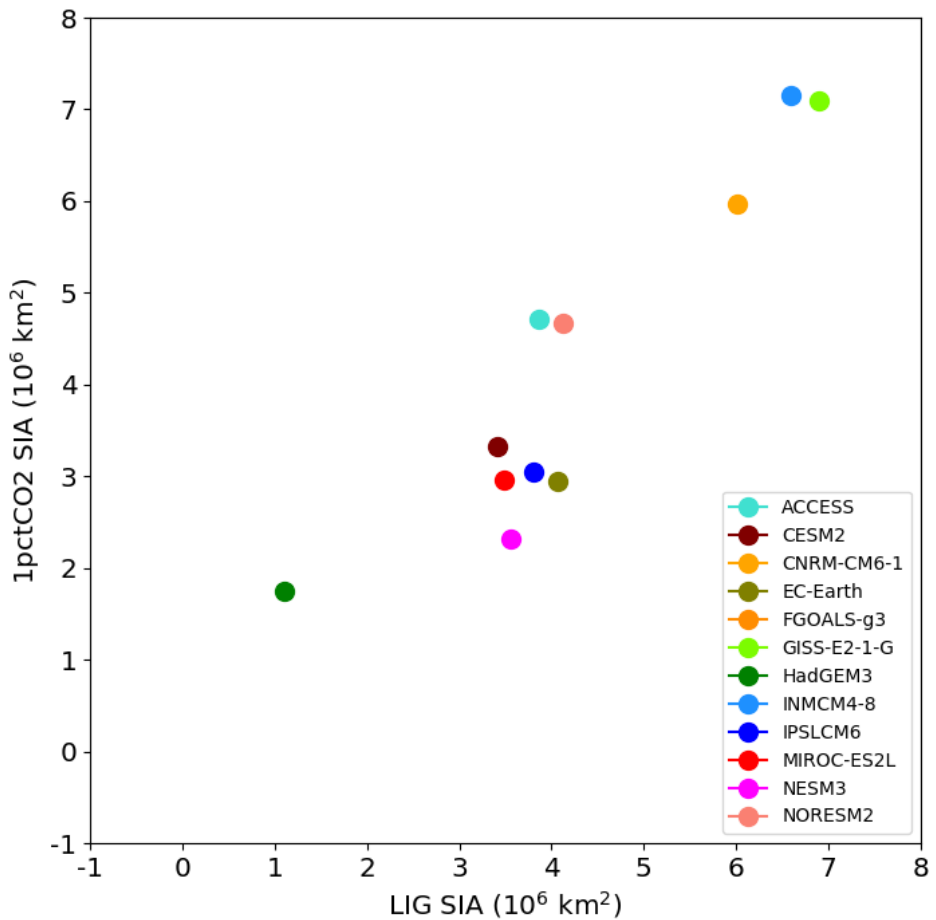


**Figure 12.** LIG vs 1pctCO<sub>2</sub> July-August-September sea ice areas (for sea ice concentrations larger than 0.15). The results for the 1pctCO<sub>2</sub> simulations have been averaged for years 50 to 70.

Adler, R. E., Polyak, L., Ortiz, J. D., Kaufman, D. S., Channell, J. E. T., Xuan, C., Grottoli, A. G., Selln, E., and Crawford, K. A.: Sediment record from the western Arctic Ocean with an improved Late Quaternary age resolution: HOTRAX core HLY0503-8JPC, Mendeleev Ridge, *Global and Planetary Change*, 68, 18–29, <https://doi.org/10.1016/j.gloplacha.2009.03.026>, 2009.

Auclair, G. and Tremblay, L. B.: The role of ocean heat transport in rapid sea ice declines in the Community Earth System Model Large Ensemble., *Journal of Geophysical Research: Oceans*, 123, 8941–8957, <https://doi.org/https://doi.org/10.1029/2018JC014525>, 2018.

Bartlein, P. J. and Shafer, S. L.: Paleo calendar-effect adjustments in time-slice and transient climate-model simulations (PaleoCalAdjust v1.0): impact and strategies for data analysis, *Geoscientific Model Development*, 12, 3889–3913, <https://doi.org/10.5194/gmd-12-3889-2019>, <https://www.geosci-model-dev.net/12/3889/2019/>, 2019.

Belt, S.: Source-specific biomarkers as proxies for Arctic and Antarctic sea ice, *Org. Geochem.*, 125, 277–298, <https://doi.org/10.1016/j.orggeochem.2018.10.002>, 2018.

Belt, S. T., Massé, G., Rowland, S. J., Poulin, M., Michel, C., and LeBlanc, B.: A novel chemical fossil of palaeo sea ice: IP25, *Organic Geochemistry*, 38, 16 – 27, <https://doi.org/https://doi.org/10.1016/j.orggeochem.2006.09.013>, <http://www.sciencedirect.com/science/article/pii/S0146638006002464>, 2007.

Belt, S. T., Cabedo-Sanz, P., Smik, L., Navarro-Rodriguez, A., Berben, S. M., Knies, J., and Husum, K.: Identification of paleo Arctic winter sea ice limits and the marginal ice zone: Optimised biomarker-based reconstructions of late Quaternary Arctic sea ice, *Earth and Planetary Science Letters*, 431, 127 – 139, <https://doi.org/https://doi.org/10.1016/j.epsl.2015.09.020>, <http://www.sciencedirect.com/science/article/pii/S0012821X15005877>, 2015.

Berger, A. and Loutre, M.-F.: Insolation values for the climate of the last 10 million years, *Quaternary Science Reviews*, 10, 297–317, 1991.

Boucher, O., Servonnat, J., Albright, A. L., Aumont, O., Balkanski, Y., Bastrikov, V., Bekki, S., Bonnet, R., Bony, S., Bopp, L., Braconnot, P., Brockmann, P., Cadule, P., Caubel, A., Cheruy, F., Cozic, A., Cugnet, D., D'Andrea, F., Davini, P., de Lavergne, C., Denvil, S., Dupont, E., Deshayes, J., Devilliers, M., Ducharne, A., Dufresne, J.-L., Ethé, C., Fairhead, L., Falletti, L., Foujols, M.-A., Gardoll, S., Gastineau, G., Ghattas, J., Grandpeix, J.-Y., Guenet, B., Guez, L., Guilyardi, E., Guimbertea, M., Hauglustaine, D., Hourdin, F., Idelkadi, A., Joussaume, S., Kageyama, M., Khadre-Traoré, A., Khodri, M., Krinner, G., Lebas, N., Levavasseur, G., Lévy, C., Lott, F., Lurton, T., Luyssaert, S., Madec, G., Madeleine, J.-B., Maignan, F., Marchand, M., Marti, O., Mellul, L., Meurdesoif, Y., Mignot, J., Musat, I., Ottlé, C., Peylin, P., Planton, Y., Polcher, J., Rio, C., Rousset, C., Sepulchre, P., Sima, A., Swingedouw, D., Thiéblemont, R., Vancoppenolle, M., Vial, J., Vialard, J., Viovy, N., and Vuichard, N.: Presentation and evaluation of the IPSL-CM6A-LR climate model, *Journal of Advances in Modeling Earth Systems*, submitted, 2019.

Brigham-Grette, J. and Hopkins, D. M.: Emergent marine record and paleoclimate of the last interglaciation along the northwest Alaskan coast, *Quaternary Research*, 43, 159–173, <https://doi.org/10.1006/qres.1995.1017>, 1995.

Brown, T., Belt, S. and Tatarek, A., and Mundy, C. J.: Source identification of the Arctic sea ice proxy IP25, *Nature Communications*, 5, 4197, <https://doi.org/https://doi.org/10.1038/ncomms5197>, 2014.

Cao, J., Wang, B., Yang, Y.-M., Ma, L., Li, J., Sun, B., Bao, Y., He, J., Zhou, X., and Wu, L.: The NUIST Earth System Model (NESM) version 3: description and preliminary evaluation, *Geoscientific Model Development*, 11, 2975–2993, <https://doi.org/10.5194/gmd-11-2975-2018>, <https://www.geosci-model-dev.net/11/2975/2018/>, 2018.

440 Capron, E., Govin, A., Feng, R., Otto-Bliesner, B. L., and Wolff, E. W.: Critical evaluation of climate syntheses to benchmark CMIP6/PMIP4 127 ka Last Interglacial simulations in the high-latitude regions, *Quaternary Science Reviews*, 168, 137–150, <https://doi.org/10.1016/j.quascirev.2017.04.019>, 2017.

445 Cronin, T., Gemery, L., Briggs Jr., W., Jakobsson, M., Polyak, L., and Brouwers, E.: Quaternary Sea-ice history in the Arctic Ocean based on a new Ostracode sea-ice proxy, *Quat. Sci. Rev.*, 29, 3415–3429, <https://doi.org/10.1016/j.quascirev.2010.05.024>, 2010.

450 Danabasoglu, G., Lamarque, J. F., Bachmeister, J., Bailey, D. A., DuVivier, A. K., Edwards, J., Emmons, L. K., Fasullo, J., Garcia, R., Gettelman, A., Hannay, C., Holland, M. M., et al.: The Community Earth System Model version 2 (CESM2), *Journal of Advances in Modeling Earth Systems*, submitted, 2019.

455 de Vernal, A. and Hillaire-Marcel, C.: Natural Variability of Greenland Climate, Vegetation and Ice Volume during the Last Million Years, *Science*, 320, 1622–1625, [https://doi.org/https://doi.org/10.1126/science.1153929](https://doi.org/10.1126/science.1153929), 2008.

460 de Vernal, A., Eynaud, F., Henry, M., Hillaire-Marcel, C., Londeix, L., Mangin, S., Matthiessen, J., Marret, F., Radi, T., Rochon, A., Solignac, S., and Turon, J.-L.: Reconstruction of sea-surface conditions at middle to high latitudes of the Northern Hemisphere, <https://doi.org/10.1594/PANGAEA.738562>, <https://doi.org/10.1594/PANGAEA.738562>, supplement to: de Vernal, A et al. (2005): Reconstruction of sea-surface conditions at middle to high latitudes of the Northern Hemisphere during the Last Glacial Maximum(LGM) based on dinoflagellate cyst assemblages. *Quaternary Science Reviews*, 24(7-9), 897-924, <https://doi.org/10.1016/j.quascirev.2004.06.014>, 2005.

465 de Vernal, A., Hillaire-Marcel, C., and Darby, D. A.: Variability of sea ice cover in the Chukchi Sea (western Arctic Ocean) during the Holocene, *Paleoceanography*, 20, <https://doi.org/https://doi.org/10.1029/2005PA001157>, 2005b.

470 de Vernal, A., Gersonde, R., Goosse, H., Seidenkrantz, M.-S., and W.Wolff, E.: Sea ice in the paleoclimate system: the challenge of reconstructing sea ice from proxies – an introduction, *Quaternary Science Reviews*, 79, 1–8, <https://doi.org/https://doi.org/10.1016/j.quascirev.2013.08.009>, 2013a.

475 de Vernal, A., Rochon, A., Fréchette, B., Henry, M., Radi, T., and Solignac, S.: Reconstructing past sea ice cover of the Northern Hemisphere from dinocyst assemblages: status of the approach, *Quaternary Science Reviews*, 79, 122–134, <https://doi.org/https://doi.org/10.1016/j.quascirev.2013.06.022>, 2013b.

480 de Vernal, A., Radi, T., Zaragosi, S., Nieuwenhove, N. V., Rochon, A., Allana, E., Scheppere, S. D., Eynaud, F., J.Head, M., Limoges, A., Londeix, L., Marret, F., Matthiessen, J., Penaud, A., Pospelova, V., Price, A., and Richerol, T.: Distribution of common modern dinoflagellate cyst taxa in surface sediments of the Northern Hemisphere in relation to environmental parameters: The new n=1968 database, *Marine Micropaleontology*, <https://doi.org/https://doi.org/10.1016/j.marmicro.2019.101796>, 2019.

485 Eynaud, F.: Kystes de Dinoflagellés et Evolution paléoclimatique et paléohydrologique de l'Atlantique Nord au cours du Dernier Cycle Climatique du Quaternaire, Ph.D. thesis, Bordeaux 1 University, 1999.

490 Eynaud, F., Turon, J., Sánchez-Goñi, M., and Gendreau, S.: Dinoflagellate cyst evidence of ‘Heinrich-like events’ off Portugal during the Marine Isotopic Stage 5, *Marine Micropaleontology*, 40, 9–21, [https://doi.org/https://doi.org/10.1016/S0377-8398\(99\)00045-6](https://doi.org/https://doi.org/10.1016/S0377-8398(99)00045-6), 2000.

495 Eynaud, F., Turon, J., and Duprat, J.: Comparison of the Holocene and Eemian palaeoenvironments in the South Icelandic Basin: dinoflagellate cysts as proxies for the North Atlantic surface circulation, *Review of Palaeobotany and Palynology*, 128, 55–79, [https://doi.org/https://doi.org/10.1016/S0034-6667\(03\)00112-X](https://doi.org/https://doi.org/10.1016/S0034-6667(03)00112-X), 2004.

500 Eyring, V., Bony, S., Meehl, G. A., Senior, C. A., Stevens, B., Stouffer, R. J., and Taylor, K. E.: Overview of the Coupled Model Intercomparison Project Phase 6 (CMIP6) experimental design and organization, *Geoscientific Model Development (Online)*, 9, 2016.

Fischer, H., Meissner, K. J., Mix, A. C., Abram, N. J., Austermann, J., Brovkin, V., Capron, E., Colombaroli, D., Daniau, A.-L., Dyez, K. A., et al.: Palaeoclimate constraints on the impact of 2C anthropogenic warming and beyond, *Nature geoscience*, 11, 474, 2018.

Goosse, H., Brovkin, V., Fichefet, T., Haarsma, R., Huybrechts, P., Jongma, J., Mouchet, A., Selten, F., Barriat, P.-Y., Campin, J.-M., Deleersnijder, E., Driesschaert, E., Goelzer, H., Janssens, I., Loutre, M.-F., Morales Maqueda, M. A., Opsteegh, T., Mathieu, P.-P., Munhoven, G., Pettersson, E. J., Renssen, H., Roche, D. M., Schaeffer, M., Tartinville, B., Timmermann, A., and Weber, S. L.: Description of the Earth system model of intermediate complexity LOVECLIM version 1.2, *Geoscientific Model Development*, 3, 603–633, <https://doi.org/10.5194/gmd-3-603-2010>, <https://www.geosci-model-dev.net/3/603/2010/>, 2010.

Guarino, M.-V., Sime, L. C., Schroeder, D., Lister, G. M. S., and Hatcher, R.: Machine dependence and reproducibility for coupled climate simulations: The HadGEM3-GC3.1 CMIP Preindustrial simulation, *Geoscientific Model Development*, 13, 139–154, <https://doi.org/10.5194/gmd-13-139-2020>, 2020.

Guo, C., Bentsen, M., Bethke, I., Ilicak, M., Tjiputra, J., Toniazzo, T., Schwinger, J., and Otterå, O. H.: Description and evaluation of NorESM1-F: a fast version of the Norwegian Earth System Model (NorESM), *Geoscientific Model Development*, 12, 343–362, 2019.

Hajima, T., Watanabe, M., Yamamoto, A., Tatebe, H., Noguchi, M. A., Abe, M., O. R., Ito, A., Yamazaki, D., Okajima, H., Ito, A., Takata, K., Ogochi, K., and Watanabe, S.: Description of the MIROC-ES2L Earth system model and evaluation of its climate–biogeochemical processes and feedbacks., *Geoscientific Model Development*, <https://doi.org/https://doi.org/10.5194/gmd-2019-275>, <https://www.geosci-model-dev-discuss.net/gmd-2019-275/>, 2019.

Hazeleger, W., Wang, X., Severijns, C., Štefănescu, S., Bintanja, R., Sterl, A., Wyser, K., Semmler, T., Yang, S., Van den Hurk, B., et al.: EC-Earth V2. 2: description and validation of a new seamless earth system prediction model, *Climate dynamics*, 39, 2611–2629, 2012.

He, M., Hu, Y., Chen, N., Wang, D., Huang, J., and Stamnes, K.: High cloud coverage over melted areas dominates the impact of clouds on the albedo feedback in the Arctic., *Scientific Reports*, 9, 9529, <https://doi.org/https://doi.org/10.1038/s41598-019-44155-w>, 2019.

Hillaire-Marcel, C., de Vernal, A., Bilodeau, G., and Weaver, A. J.: Absence of deep-water formation in the Labrador Sea during the last interglacial period, *Nature*, 410, 1073–1077, 2001.

Hillaire-Marcel, C., Ghaleb, B., de Vernal, A., Maccalli, J., Cuny, K., Jacobel, A., Duc, C. L., and McManus, J.: A new chronology of late quaternary sequences from the central Arctic Ocean based on “extinction ages” of their excesses in  $^{231}\text{Pa}$  and  $^{230}\text{Th}$ ., *Geochemistry, Geophysics, Geosystems*, 18, 4573–4585, <https://doi.org/https://doi.org/10.1002/2017GC007050>, 2017.

IPCC: Climate Change 2007: The Physical Science Basis. Contribution of Working Group I to the Fourth Assessment Report of the Intergovernmental Panel on Climate Change [Solomon, S., D. Qin, M. Manning, Z. Chen, M. Marquis, K.B. Averyt, M. Tignor and H.L. Miller (eds.)], Tech. Rep. 4, Intergovernmental Panel on Climate Change, Cambridge University Press, Cambridge, United Kingdom and New York, USA., 2007.

IPCC: Climate Change 2013: The Physical Science Basis. Contribution of Working Group I to the Fifth Assessment Report of the Intergovernmental Panel on Climate Change. [Stocker, T.F. and Qin, D and Plattner, G and Tignor, M and Allen, S.K. and Boschung, J and Nauels, A and Xia, Y and Bex, V and Midgley, P.M (eds.)], Tech. Rep. 5, Intergovernmental Panel on Climate Change, Cambridge, United Kingdom and New York, NY, USA, <https://doi.org/10.1017/CBO9781107415324>, 2013.

Kageyama, M., Braconnot, P., Harrison, S. P., Haywood, A. M., Jungclaus, J. H., Otto-Bliesner, B. L., Peterschmitt, J.-Y., Abe-Ouchi, A., Albani, S., Bartlein, P. J., Brierley, C., Crucifix, M., Dolan, A., Fernandez-Donado, L., Fischer, H., Hopcroft, P. O., Ivanovic, R. F., Lambert, F., Lunt, D. J., Mahowald, N. M., Peltier, W. R., Phipps, S. J., Roche, D. M., Schmidt, G. A., Tarasov, L., Valdes, P. J., Zhang, Q., and Zhou, T.: The PMIP4 contribution to CMIP6 – Part 1: Overview and over-arching analysis plan, *Geoscientific Model Development*, 11, 1033–1057, <https://doi.org/10.5194/gmd-11-1033-2018>, <https://www.geosci-model-dev.net/11/1033/2018/>, 2018.

515 Kelley, M., Schmidt, G. A., Nazarenko, L., Miller, R. L., Bauer, S. E., Ruedy, R., Russell, G. L., Aleinov, I., Bauer, M., Bleck, R., Canuto, V., Cesana, G., Cheng, Y., Clune, T. L., Cook, B., Cruz, C. A., Del Genio, A. D., Elsaesser, G. S., Faluvegi, G., Kiang, N. Y., Kim, D., Lacis, A. A., Leboissetier, A., LeGrande, A. N., Lo, K. K., Marshall, J. C., McDermid, S., Matthews, E. E., Mezuman, K., Murray, L. T., Oinas, V., Orbe, C., Pérez García-Pando, C., Perlitz, J., Puma, M., Rind, D., Romanou, A., Shindell, D. T., Sun, S., Tausnev, N., Tsigaridis, K., Tselioudis, G., Weng, E., Wu, J., and Yao, M.-S.: GISS-E2.1.

520 Kremer, A., Stein, R., Fahl, K., Bauch, H., Mackensen, A., and Niessen, F.: A 190-ka biomarker record revealing interactions between sea ice, Atlantic Water inflow and ice sheet activity in eastern Fram Strait, *arktos*, 4, <https://doi.org/https://doi.org/10.1007/s41063-018-0052-0>, 2018a.

Kremer, A., Stein, R., Fahl, K., Ji, Z., Yang, Z., Wiers, S., Matthiessen, J., Forwick, M., Löwemark, L., O'Regan, M., Chen, J., and Snowball, I.: Changes in sea ice cover and ice sheet extent at the Yermak Plateau during the last 160 ka – Reconstructions from biomarker records, 525 *Quaternary Science Reviews*, 182, 93–108, <https://doi.org/https://doi.org/10.1016/j.quascirev.2017.12.016>Get rights and content, 2018b.

Lunt *et al.*, D. J.: A multi-model assessment of last interglacial temperatures, *Climate of the Past*, 9, 699–717, <https://doi.org/10.5194/cp-9-699-2013>, <http://www.clim-past.net/9/699/2013/>, 2013.

530 Malmierca-Vallet, I., Sime, L. C., Valdes, P. J., Capron, E., Vinther, B. M., and Holloway, M. D.: Simulating the Last Interglacial Greenland stable water isotope peak: The role of Arctic sea ice changes, *Quaternary Science Reviews*, 198, 1–14, <https://doi.org/doi.org/10.1016/j.quascirev.2018.07.027>, 2018.

Masson-Delmotte, V., Braconnot, P., Hoffmann, G., Jouzel, J., Kageyama, M., L. A., Lejeune, a. Q., Risi, C., Sime, L. C., Sjolte, J., Swingedouw, D., and Vinther, B. M.: Sensitivity of interglacial Greenland temperature and  $\delta^{18}\text{O}$ : ice core data, orbital and increased  $\text{CO}_2$  climate simulations, *Climate of the Past*, 7, 1041–1059, <https://doi.org/10.5194/cp-7-1041-2011>, 2011.

Matthiessen, J. and Knies, J.: tbc, tbc, tbc, tbc, <https://doi.org/tbc>, 2001.

535 Matthiessen, J., Knies, J., Nowaczyk, N. R., and Ruediger, S.: Age determination of sediment core PS2138-1, <https://doi.org/https://doi.org/10.1594/PANGAEA.728133>, supplement to: Matthiessen, J *et al.* (2001): Late Quaternary dinoflagellate cyst stratigraphy at the Eurasian continental margin, Arctic Ocean: Indications for Atlantic water inflow in the past 150,000 years. *Global and Planetary Change*, 31(1-4), 65–86, [https://doi.org/10.1016/S0921-8181\(01\)00113-8](https://doi.org/10.1016/S0921-8181(01)00113-8), 2001.

Müller, J., Wagner, A., Fahl, K., Stein, R., Prange, M., and Lohmann, G.: Towards quantitative sea ice reconstructions in the northern North Atlantic: A combined biomarker and numerical modelling approach, *Earth and Planetary Science Letters*, 306, 137 – 148, 540 <https://doi.org/https://doi.org/10.1016/j.epsl.2011.04.011>, <http://www.sciencedirect.com/science/article/pii/S0012821X11002275>, 2011.

Nørgaard-Pedersen, N., Mikkelsen, N., Lassen, S. J., Kristoffersen, Y., and Sheldon, E.: Reduced sea ice concentrations in the Arctic Ocean during the last interglacial period revealed by sediment cores off northern Greenland, *Paleoceanography*, 22, PA1218, <https://doi.org/10.1029/2006PA001283>, 2007.

545 Olonscheck, D., Mauritsen, T., and Notz, D.: Arctic sea-ice variability is primarily driven by atmospheric temperature fluctuations., *Nature Geoscience*, 12, 430–434, <https://doi.org/https://doi.org/10.1038/s41561-019-0363-1>, 2019.

Otto-Bliesner, B. L., Marshall, S. J., Overpeck, J. T., Miller, G. H., Hu, A., and members, C. L. I. P.: Simulating Arctic Climate Warmth and Icefield Retreat in the Last Interglaciation, *Science*, 311, 1751–1753, <https://doi.org/10.1126/science.1120808>, 2006.

Otto-Bliesner, B. L., Rosenbloom, N., Stone, E. J., McKay, N. P., Lunt, D. J., Brady, E. C., and Overpeck, J. T.: How warm was the last 550 interglacial? New model–data comparisons, *Philosophical Transactions of the Royal Society of London A: Mathematical, Physical and Engineering Sciences*, 371, 20130097+, <https://doi.org/10.1098/rsta.2013.0097>, <http://dx.doi.org/10.1098/rsta.2013.0097>, 2013.

Otto-Bliesner, B. L., Braconnot, P., Harrison, S. P., Lunt, D. J., Abe-Ouchi, A., Albani, S., Bartlein, P. J., Capron, E., Carlson, A. E., Dutton, A., et al.: The PMIP4 contribution to CMIP6—Part 2: Two interglacials, scientific objective and experimental design for Holocene and Last Interglacial simulations, *Geoscientific Model Development*, 10, 3979–4003, 2017.

555 Otto-Bliesner, B. L., Brady, E. C., Zhao, A., Brierley, C., Axford, Y., Capron, E., Govin, A., Hoffman, J., Isaacs, E., Kageyama, M., Scussolini, P., Tzedakis, P. C., Williams, C., Wolff, E., Abe-Ouchi, A., Braconnot, P., Ramos Buarque, S., Cao, J., de Vernal, A., Guarino, M. V., Guo, C., LeGrande, A. N., Lohmann, G., Meissner, K., Men viel, L., Nisancioglu, K., O’ishi, R., Salas Y Melia, D., Shi, X., Sicard, M., Sime, L., Tomas, R., Volodin, E., Yeung, N., Zhang, Q., Zhang, Z., and Zheng, W.: Large-scale features of Last Interglacial climate: Results from evaluating the *lig127k* simulations for CMIP6-PMIP4, *Climate of the Past Discussions*, 2020, 1–41, <https://doi.org/10.5194/cp-2019-174>, 2020. <https://www.clim-past-discuss.net/cp-2019-174/>, 2020.

560 Penaud, A., Eynaud, F., Turon, J., Zaragosi, S., Marret, F., and Bourillet, J.: Interglacial variability (MIS 5 and MIS 7) and dinoflagellate cyst assemblages in the Bay of Biscay (North Atlantic), *Marine Micropaleontology*, 68, 136–155, [https://doi.org/https://doi.org/10.1016/j.marmicro.2008.01.007](https://doi.org/10.1016/j.marmicro.2008.01.007), 2008.

565 Reynolds, R. W., Rayner, N. A. and Smith, T. M., C., S. D., and Wang, W.: An improved in situ and satellite SST analysis for climate., *J. Climate*, 15, 1609–1625, 2002.

570 Seland, Ø., Bentsen, M., Olivie, D., Tonazzo, T., Gjermundsen, A., Seland Graff, L., Debernard, J., Kumar Gupta, A., He, Y., Kirkevåg, A., Schwinger, J., Tjiputra, J., Schancke Aas, K., Bethke, I., Fan, Y., Griesfeller, J., Grini, A., Guo, C., Heinze, C., Ilicak, M., Haf-sahl Karset, I. H., Landgren, O., Liakka, J., Onsum Moseid, K., Nummelin, A., Spensberger, C., Tang, H., Zhang, Z., Iverson, T., and Schulz, M.: The Norwegian Earth System Model, NorESM2 - Evaluation of the CMIP6 DECK and historical simulations, *Geoscientific Model Development*, p. submitted, 2019.

575 Sidorenko, D., Rackow, T., Jung, T., Semmler, T., Barbi, D., Danilov, S., Dethloff, K., Dorn, W., Fieg, K., Gößling, H. F., et al.: Towards multi-resolution global climate modeling with ECHAM6–FESOM. Part I: model formulation and mean climate, *Climate Dynamics*, 44, 757–780, 2015.

Sidorenko, D., Goessling, H., Koldunov, N., Scholz, P., Danilov, S., Barbi, D., Cabos, W., Gurses, O., Harig, S., Hinrichs, C., Juricke, S., Lohmann, G., Losch, M., Mu, L., Rackow, T., Rakowsky, N., Sein, D., Semmler, T., Shi, X., Stepanek, C., Streffing, J., Wang, Q., Wekerle, C., Yang, H., and Jung, T.: Evaluation of FESOM2.0 Coupled to ECHAM6.3: Preindustrial and HighResMIP Simulations, *Journal of Advances in Modeling Earth Systems*, 11, 3794–3815, <https://doi.org/10.1029/2019MS001696>, <https://agupubs.onlinelibrary.wiley.com/doi/abs/10.1029/2019MS001696>, 2019.

580 Sime, L. C., Risi, C., Tindall, J. C., Sjolte, J., Wolff, E. W., Masson-Delmotte, V., and Capron, E.: Warm climate isotopic simulations: what do we learn about interglacial signals in Greenland ice cores?, *Quaternary Science Reviews*, 67, 59–80, <https://doi.org/10.1016/j.quascirev.2013.01.009>, <http://dx.doi.org/10.1016/j.quascirev.2013.01.009>, 2013.

SIMIP Community: Arctic Sea Ice in CMIP6, *Geophysical Research Letters*, 47, e2019GL086749, <https://doi.org/10.1029/2019GL086749>, <https://agupubs.onlinelibrary.wiley.com/doi/abs/10.1029/2019GL086749>, e2019GL086749 10.1029/2019GL086749, 2020.

585 Smik, L., Belt, S. T., Lieser, J. L., Armand, L. K., and Leventer, A.: Distributions of highly branched isoprenoid alkenes and other algal lipids in surface waters from East Antarctica: Further insights for biomarker-based paleo sea-ice reconstruction, *Organic Geochemistry*, 95, 71 – 80, [https://doi.org/https://doi.org/10.1016/j.orggeochem.2016.02.011](https://doi.org/10.1016/j.orggeochem.2016.02.011), <http://www.sciencedirect.com/science/article/pii/S0146638016000498>, 2016.

Stein, R., Fahl, K., Gierz, P., Niessen, F., and Lohmann, G.: Arctic Ocean sea ice cover during the penultimate glacial and the last interglacial, *Nature communications*, 8, <https://doi.org/10.1038/s41467-017-00552-1>, 2017.

590 Tatebe, H., Tanaka, Y., Komuro, Y., and Hasumi, H.: Impact of deep ocean mixing on the climatic mean state in the Southern Ocean., *Sci. Rep.*, 8, 14 479, <https://doi.org/doi:10.1038/s41598-018-32768-6>, 2018.

Van Nieuwenhove, N. and Bauch, H. A.: Last interglacial (MIS 5e) surface water conditions at the VPlateau (Norwegian Sea), based on dinoflagellate cysts, *Polar Research*, 27, 175–186, <https://doi.org/https://doi.org/10.3402/polar.v27i2.6175>, 2008.

Van Nieuwenhove, N., Bauch, H. A., and Matthiessen, J.: Last interglacial surface water conditions in the eastern 595 Nordic Seas inferred from dinocyst and foraminiferal assemblages, *Marine Micropaleontology*, 66, 247–263, <https://doi.org/https://doi.org/10.1016/j.marmicro.2007.10.004>, 2008.

Van Nieuwenhove, N., Bauch, H. A., Eynaud, F., Kandiano, E., Cortijo, E., and Turon, J.-L.: Evidence for delayed poleward 600 expansion of North Atlantic surface waters during the last interglacial (MIS 5e), *Quaternary Science Reviews*, 30, 934–946, <https://doi.org/https://doi.org/10.1016/j.quascirev.2011.01.013>, 2011.

Van Nieuwenhove, N., Bauch, H. A., and Andrleit, H.: Multiproxy fossil comparison reveals contrasting surface ocean 605 conditions in the western Iceland Sea for the last two interglacials, *Palaeogeography, Palaeoclimatology, Palaeoecology*, 370, 247–259, <https://doi.org/https://doi.org/10.1016/j.palaeo.2012.12.018>, 2013.

Vaughan, D., Comiso, J., Allison, I., Carrasco, J., Kaser, G., Kwok, R., Mote, P., Murray, T., Paul, F., Ren, J., Rignot, E., Solomina, O., 610 Steffen, K., and Zhang, T.: Observations: Cryosphere, in: *Climate Change 2013: The Physical Science Basis. Contribution of Working Group I to the Fifth Assessment Report of the Intergovernmental Panel on Climate Change*, edited by Stocker, T., Qin, Plattner, G.-K., Tignor, M., Allen, S.K. and Boschung, J., Nauels, A., Xia, Y., Bex, V., and Midgley, P., Cambridge University Press, 2013.

Volodko, A., Saint-Martin, D., Sénési, S., Decharme, B., Alias, A., Chevallier, M., Colin, J., G. J. F., Michou, M., Moine, M.-P., and Nabat, P.: Evaluation of CMIP6 DECK Experiments With CNRM-CM6.1, *Journal of Advances in Modeling Earth Systems*, 11, 2177–2213, <https://doi.org/10.1029/2019M01029>, 2019.

Volodin, E. M., Mortikov, E. V., Kostrykin, S. V., Galin, V. Y., Lykossov, V. N., Gritsun, A. S., Diansky, N. A., Gusev, A. V., Iakovlev, N. G., Shestakova, A. A., et al.: Simulation of the modern climate using the INM-CM48 climate model, *Russian Journal of Numerical Analysis and Mathematical Modelling*, 33, 367–374, 2018.

Walsh, J. E., Chapman, W. L., and Fetterer, F.: Gridded Monthly Sea Ice Extent and Concentration, 1850 Onward, Version 1, <https://doi.org/doi: https://doi.org/10.7265/N5833PZ5>, 2016.

Williams, K., Copsey, D., Blockley, E., Bodas-Salcedo, A., Calvert, D., Comer, R., Davis, P., Graham, T., Hewitt, H., Hill, R., et al.: The 615 Met Office global coupled model 3.0 and 3.1 (GC3. 0 and GC3. 1) configurations, *Journal of Advances in Modeling Earth Systems*, 10, 357–380, 2018.

Xiao, X., Stein, R., and Fahl, K.: MIS 3 to MIS 1 temporal and LGM spatial variability in Arctic Ocean sea ice cover: Reconstruction from biomarkers, *Paleoceanography*, 30, 969–983, 2015.

Ziehn, T., Lenton, A., Law, R. M., Matear, R. J., and Chamberlain, M. A.: The carbon cycle in the Australian Community Climate and Earth 620 System Simulator (ACCESS-ESM1)-Part 2: Historical simulations., *Geoscientific Model Development*, 10, 2017.